

Chapter 2

Theory and Computational Techniques

This chapter is dedicated to the explanation of all the technical details regarding the simulation methods we used in this work. It is meant to supply a sound description of these methods, but for a deeper understanding we refer to the literature [All87, Fre96, Pan88, Pan00, Eva89, Eva90, Hey98]. The actual implementation of the algorithms can be found elsewhere [All87, Sad99, Fre96, Eva84a]. However in Appendix 2 we report the algorithm for three-body forces, because to the best of our knowledge, it has not been given previously in the literature.

We give details of the intermolecular potentials used to study argon, krypton and xenon, in both equilibrium and non-equilibrium simulations reported here. We draw particular attention to the three-body potentials, since they represent the focus of our investigation. We introduce the Gibbs ensemble Monte Carlo technique that is used to investigate the vapour-liquid phases of the noble gases. The general concepts of non-equilibrium systems are discussed, in order to explain the algorithms used to implement planar Couette flow simulations.

2.1 Intermolecular potentials

In this work we study properties of the noble gases argon, krypton and xenon with realistic potentials, the predictions of which have been extensively proved to be in good

agreement with experimental results. The remaining stable noble gases, helium and neon, were not considered because of uncertainties arising from quantum effects. Some molecular dynamics studies and *ab initio* calculations for helium and neon have been reported recently [Azi95, Erl98, Kir98]. Several accurate intermolecular potentials are available in the literature [Mai81] for argon, krypton and xenon. We have chosen to use the intermolecular two-body potentials proposed by Barker et al. [Bar71a, Bar74] and three-body potentials proposed by Axilrod-Teller [Axi43] and Bell [Bel71], because of their well-known accuracy and the availability of intermolecular potential parameters for argon, krypton and xenon. A recent review of intermolecular potentials is available elsewhere [Sad99].

In section 2.1.1 we introduce briefly the Born-Oppenheimer approximation, which is commonly adopted in relation to intermolecular potentials. In section 2.1.2 we give details of the two-body potentials used. In section 2.1.3 a short review on three-body potentials is given.

2.1.1 Born-Oppenheimer approximation

An intermolecular potential function can be derived from quantum mechanical calculations or from experimental data fits, or from both. In general it requires the use of the *Born-Oppenheimer approximation* [Dob57]: if H is the total Hamiltonian of an atomic or molecular system and \mathbf{Y} the total wave function, the state of the nuclei and the electrons can be obtained from the Schroedinger equation:

$$H\mathbf{Y} = E\mathbf{Y} \quad (2.1)$$

where E is the total energy. H is the sum of the kinetic energy of the nuclei T_n , the kinetic energy of the electrons T_e and the electrostatic potential energy U :

$$H\mathbf{Y} = (T_n + T_e + U)\mathbf{Y} = E\mathbf{Y} \quad . \quad (2.2)$$

In a real system, since the velocity of the nuclei is much slower than the velocity of the electrons, T_n is much smaller than T_e . For this reason the state of the electrons can be derived adopting the approximation that the nuclei are fixed. This assumption enables one to write the total wave function \mathbf{Y} as a product of a first function, \mathbf{c} , depending only on the nuclei coordinates, and a second function, \mathbf{f} , depending on the electron coordinates and depending on nuclei positions in a parametric way:

$$\mathbf{Y} = \mathbf{c}(x_n) \mathbf{f}(x_n, x_e) \quad (2.3)$$

where x_e are the electron coordinates and x_n are the nuclei positions. Considering the nuclei fixed, the Schroedinger equation for the electrons becomes:

$$(T_e + U) \mathbf{f}(x_n, x_e) = E \mathbf{f}(x_n, x_e) \quad (2.4)$$

Both the energy E and the wave functions $\mathbf{f}(x_n, x_e)$ depend on the configuration x_n of the nuclei, so changing x_n as a parameter changes the energy and the wave function. For many condensed systems, given the nuclei configuration x'_n , the electrons remain in the lowest energy level (ground state) $E_o(x'_n)$ for a wide range of temperature and pressure values. Hence, for any configuration (x_n, x_e) it is possible to use the relative ground state eigenvalue $E_o(x_n)$ to write the Schroedinger equation for the nuclei:

$$(T_n + E_o(x_n)) \mathbf{c}(x_n) = E \mathbf{c}(x_n) \quad (2.5)$$

In this way $E_o(x_n)$ has the role of an intermolecular potential, $u(x_n)$, to be determined by theoretical calculations or by experimental data. The Born-Oppenheimer approximation (or adiabatic approximation) states that the electrons are moving as though the nuclei were fixed in their instantaneous positions. The nuclear motion only deforms the electronic ground state; electronic transitions from the ground state to excited ones are excluded. This approximation is applicable to the noble gases [Bor54].

The intermolecular potential $u(x_n)$ in the absence of external forces may in general be written as function of the nuclear coordinates $r_1 \dots r_N$ as [Bel76]:

$$u(r_1, \dots, r_N) = \sum_{i < j}^N u_2(r_i, r_j) + \sum_{i < j < k}^N u_3(r_i, r_j, r_k) + \dots \quad (2.6)$$

where u_2 , $u_3 \dots$ are respectively pair, triplet, etc. potential functions. Experimental evidence [Bar76] indicates that this series is rapidly convergent and for many measurable properties the pairwise additive approximation (u_2 term only) is a valid description. In principle the pairwise additive approximation is inconsistent, since any quantum mechanical estimate of the pair potential u_2 must include effects due to higher terms (u_3 , $u_4 \dots$) [Ege94]. The wide use of the pairwise additive approximation is motivated by its simplicity. Furthermore, the above inconsistency is overcome by using effective potentials, namely, two-body potentials that accounts for the overall effects of the other multi-body interactions. The Lennard-Jones potential [Mai81, All87, Sad99] is an example of an effective two-body potential since its parameters are evaluated from bulk experimental data which include many-body effects. In our work, focused on the noble gases argon, krypton and xenon, we intend to study the role of three-body potentials (u_3), used in conjunction with an authentic two-body potential (u_2), making the assumption that higher order terms are negligible.

2.1.2 Two-body intermolecular potential

Information to determine the intermolecular potential

The general shape of the intermolecular potential function for a noble gas dimer is known. To acquire detailed information on different regions of this function, several types of experiments may be used. To achieve this task three conditions must be satisfied, as Barker pointed out [Bar76]:

- 1) *the experimental quantity must depend reasonably sensitively on some feature of the potential;*
- 2) *it must be possible to measure the quantity with sufficient accuracy;*
- 3) *adequate theory and computational procedures must exist to permit calculation of the experimental quantity from a given potential or, preferably, of the potential from the experimental quantity.*

Quantum mechanics calculations can be used to accurately determine the short-range repulsion part of the potential [Mur76] (Hartre-Fock and multi-configuration Hartre-Fock calculations). This short-range contribution arises from the overlap of the electron wave functions of two atoms. It is a rapidly varying function of the interatomic distance and is usually represented as an exponential function or as an inverse high power of the interatomic distance [Mur76]. Important information on the repulsion part of the potential comes from molecular beam scattering experiments that allow high-energy total cross-section measurements [Bar76].

For the long-range attraction part (dispersion or van der Waals forces) second-order perturbation theory [Bra83, van98] provides an asymptotic form:

$$u'(r) = -\frac{C_6}{r^6} - \frac{C_8}{r^8} - \frac{C_{10}}{r^{10}} \dots \quad (2.7)$$

where r is the interatomic distance and the coefficients C_6 , C_8 and C_{10} are related to the dipole and multipole oscillator strengths which can be measured from optical properties [Leo75]. The dispersion forces follow from the correlation between the fluctuating charge densities of the two atoms and they are largely independent of the overlap of the electron wave functions of the two atoms [Mur76]. In particular, the term in r^{-6} depends

on the fluctuating dipole-dipole interaction, the term in r^{-8} on the dipole-quadrupole interaction, and so on.

Van der Waals forces in inert gases enable the formation of bound states (dimers); it is possible to observe and measure band systems [Tan70] due to transitions from ground electronic states to excited electronic states of these dimers. These measurements provide information about the curvature at the potential minimum and about the anharmonicity of the potential [Bar76]. Other information on the potential function comes from gas transport properties such as viscosity, thermal conductivity, diffusion coefficients, thermal diffusion ratio and second virial coefficient [Bar76].

All the kinds of measurement discussed so far depend only on the two-body potential. For example, the second virial coefficient, B , from the equation of state

$$\frac{PV}{RT} = 1 + \frac{B}{V} + \frac{C}{V^2} + \dots \quad (2.8)$$

is related to the potential by the *classical* relationship [All87]:

$$B = \frac{2pN}{3} \int_0^{\infty} \left(e^{-\frac{u(r)}{kT}} - 1 \right) r^2 dr \quad (2.9)$$

It is possible to show with the Wigner-Kirkwood [Bar71a] expansion of the partition function that the quantum contributions to the second virial coefficient for argon, krypton and xenon can be neglected.

The third virial coefficient depends on both two-body and three-body potentials, and it has been shown [Bar76 and Bar68] that the inclusion of a three-body interaction, such as the Axilrod-Teller term [Axi43], can improve significantly the agreement between the calculated value and the experimental one. The same approach has to be used with condensed phase data where three-body effects are important.

The solid state, in particular the crystal structure, provides additional useful information [Bar76]. The sublimation energy at 0 K depends significantly on the depth of the minimum of the two-body potential. The lattice parameter depends on the distance where the potential has a minimum. The bulk modulus near 0 K is closely proportional to the second derivative of the potential at its minimum, and the 0 K Debye parameter to the square root of the same quantity. The low-temperature thermal expansion coefficient is related to the third derivative of the potential near its minimum. It is particularly noteworthy that most of the pair potentials for noble gases predict the hexagonal close-packed (hcp) crystal as the most stable structure, while noble gases crystallize in face-centred cubic (fcc) structures. It has been suggested that the use of many-body potentials can instead favor the cubic structure [Nie76, Lot97a].

Liquid state properties give the opportunity to test the potential, comparing experimental values of quantities such as pressure with calculated values obtained with *Monte Carlo* and *molecular dynamics* techniques. With the same techniques it is possible to calculate the radial distribution function $g(r)$ and compare it with the one determined from X-ray and neutron diffraction data.

Argon

Most of the techniques to derive intermolecular potentials were applied to argon since a large collection of experimental data was available. An equivalent amount of data is accessible for helium but quantum effects are now important and make the calculation more difficult. In the literature several intermolecular potentials for argon were proposed [Mai81, Sad99, Azi93]. We decided to use the two-body potential by Barker, Fisher and Watts (BFW) [Bar71a] for its accuracy and also since similar analytic expressions are available for other noble gases (krypton and xenon [Bar74]).

The BFW potential is a true two-body potential since it was derived only by properties depending on two-body interactions.

The BFW potential is a linear combination of the Barker-Pompe [Bar68] (u_{BP}) and Bobetic-Barker [Bob70] (u_{BB}) potentials:

$$u_2(r) = 0.75u_{BB}(r) + 0.25u_{BP}(r) \quad (2.10)$$

where the potentials of Barker-Pompe and Bobetic-Barker have the following form:

$$u(r) = e \left[\sum_{i=0}^5 A_i (x-1)^i \exp[\mathbf{a}(1-x)] - \sum_{j=0}^2 \frac{C_{2j+6}}{\mathbf{d} + x^{2j+6}} \right]. \quad (2.11)$$

In Eq. (2.11), $x = r/r_m$ where r_m is the intermolecular separation at which the potential has a minimum value. The other parameters are summarised in Table 2.1:

Table 2.1 Parameters of the Barker-Pompe [Bar68], Bobetic-Barker [Bob70] and Barker-Fisher-Watts (BFW) [Bar71a] potentials.

	Barker-Pompe	Bobetic-Barker	Barker-Fisher-Watts
$e/k(K)$	147.70	140.235	142.095
$\mathbf{s}(\text{\AA})$	3.7560	3.7630	3.3605
$r_m(\text{\AA})$	3.341	3.3666	3.7612
A_0	0.2349	0.29214	0.27783
A_1	-4.7735	-4.41458	-4.50431
A_2	-10.2194	-7.70182	-8.331215
A_3	-5.2905	-31.9293	-25.2696
A_4	0.0	-136.026	-102.0195
A_5	0.0	-151.0	-113.25
C_6	1.0698	1.11976	1.10727
C_8	0.1642	0.171551	0.16971325
C_{10}	0.0132	0.013748	0.013611
\mathbf{a}	12.5	12.5	12.5
\mathbf{d}	0.01	0.01	0.01

The BFW potential can be written as in Eq. (2.11) with the potential parameters taken from the 4th column of Table 2.1. The \mathbf{s} term is the value where the potential is zero and it is usually defined as the atomic diameter.

Barker et al. [Bar71a] used the following experimental data to determine the potential:

- 1) high-energy molecular beam data;
- 2) the zero-temperature and -pressure lattice spacing, energy and Debye parameter, derived from specific heat measurements of solid argon;
- 3) the known long-range coefficients of r^{-6} , r^{-8} and r^{-10} ;
- 4) second virial coefficients;
- 5) the liquid-phase pressure at one temperature and density;
- 6) the known coefficient of the Axillord-Teller interaction [Axi43].

The BFW potential used with Axilrod-Teller three-body interactions was demonstrated to be in good agreement with several experimental properties of argon [Bar71a]. These include pressure and internal energy of the liquid state, solid state properties (specific heat, pressure), zero-shear viscosity, thermal diffusion ratio and molecular beam scattering data. Contributions from third-order dipole-quadrupole and fourth-order triple-dipole interactions cancel each other almost completely in condensed phase proprieties of argon [Bar72a and Mar99].

Krypton and xenon

The molecule-specific nature of the BFW potential is illustrated by attempts to use Eq. (2.11) for other noble gases such as krypton and xenon. Barker et al. [Bar74] reported that modifications to Eq. (2.11) were required to obtain an optimal representation for these larger noble gases. For krypton and xenon, they determined a potential of the form:

$$u_2(r) = u_0(r) + u_1(r) \quad (2.12)$$

where $u_0(r)$ is identical to Eq. (2.11) and $u_1(r)$ is given by

$$u_1(r) = \begin{cases} \mathbf{e} [P(x-1)^4 + Q(x-1)^5] \exp[\mathbf{a}'(1-x)] & x > 1 \\ 0 & x \leq 1 \end{cases} \quad (2.13)$$

and \mathbf{a}' , P and Q are additional parameters obtained by fitting data for differential scattering cross-sections. We have used Eqs. (2.12) and (2.13) to calculate the properties of krypton and xenon with the parameters [Bar74] summarised in Table 2.2. It is important to stress that $u_1(r)$ in Eq. (2.13) is continuous everywhere together with its first three derivatives and has a long-range asymptotic behavior.

Table 2.2 Parameters of the two-body potentials for krypton and xenon [Bar74].

	krypton	xenon
$\mathbf{e}k(K)$	201.9	281.0
$\mathbf{s}(A)$	3.573	3.890
$r_m(A)$	4.0067	4.3623
A_0	0.23526	0.2402
A_1	-4.78686	-4.8169
A_2	-9.2	-10.9
A_3	-8.0	-25.0
A_4	-30.0	-50.7
A_5	-205.8	-200.0
C_6	1.0632	1.0544
C_8	0.1701	0.1660
C_{10}	0.0143	0.0323
P	-9.0	59.3
Q	68.67	71.1
\mathbf{a}	12.5	12.5
\mathbf{a}'	12.5	12.5
\mathbf{d}	0.01	0.01

The experimental data used to derive these potentials were [Bar74]:

- 1) lattice spacing and cohesive energy of the crystal at 0 K;
- 2) bulk modulus and Debye parameter at 0 K;
- 3) lower vibrational level spacings derived from spectroscopic data;
- 4) gas viscosity data;
- 5) differential scattering cross sections;

6) second virial coefficients.

For krypton all these data turned out to be consistent. For xenon the depth of the potential, ϵ , had to be changed from the value suggested by the cohesive energy [Bar74]. In Table 2.3 some solid state proprieties at 0 K are compared with values calculated using the potentials from Baker et al. [Bar74]. The comparison indicates relatively good agreement supporting the accuracy of the potentials.

Table 2.3 Solid state proprieties at 0 K compared with values calculated using the potentials from Baker et al [Bar74].

	Nearest- neighbour distance (\AA)	Cohesive energy (cal/mol)	Bulk modulus (kbar)	Debye parameter Q (K)
Experimental Kr	3.9922	-2666	34.3	71.9
Calculated Kr	3.9917	-2665	35.7	71.1
Experimental Xe	4.3357	-3830	36.5	64.0
Calculated Xe	4.3355	-3754	38.2	60.9

2.1.3 Many-body potentials

Modern developments in experimental techniques and computing technology have allowed an increase in the interest and the effort towards understanding many-body effects. More accurate knowledge of the 2-body potential and access to new experimental and theoretical methods has encouraged many researchers to investigate higher many-body effects, which are necessary to describe macroscopic proprieties from a microscopic viewpoint. For a comprehensive survey on this topic we refer to the review of Elrod and Saykally [Elr94]; here we intend to highlight the most important and established aspects in order to explain and justify the use of the 3-body potential functions we have chosen.

Many-body effects in any system are usually at least one order of magnitude smaller than the two-body effects, hence, any investigation on this topic requires the knowledge of an accurate two-body potential. Noble gases satisfied this requirement and consequently they were the first system studied in this context.

Even neutral atoms, with spherical charge distributions, are characterized by long-range interactions. When atoms are brought in close proximity, the instantaneous interaction between the electrons in their orbits induces mutual polarization of the charge distributions. Usually, this effect is envisaged in terms of multipole components, dipole (D), quadrupole (Q), octopole (O) etc., in the perturbed charge distributions [Bel76]. In 1943 Axilrod and Teller [Axi43], using third-order perturbation theory, found the expression for the three-body triple-dipole long-range (dispersion) energy (DDD or AT term), valid for atoms with spherical and non-overlapping charge distributions [Mur76]. In 1970, Bell [Bel70] found a more general long-range (dispersion) third-order potential:

$$u_{3bodyDisp} = DDD + DDQ + DQQ + QQQ \quad (2.14)$$

Doran and Zucker [Dor71] used these terms plus the third-order dipole-dipole-octupole and fourth-order third-dipole to investigate the preferred crystal structure of the noble gases. They found again that this was the hcp lattice and not the fcc as experimental data show.

The effect of short-range many-body forces has not been investigated as deeply as the many-body dispersion. As for the two-body case, short-range many-body effects originate from the overlap of the wave functions of the atoms (triplets, quadruplets etc.) [Mur76]. When the overlap of the wave functions is not negligible the exchange forces due to the Pauli exclusion principle [Bra83] become relevant. Unfortunately, the derivation of higher-order exchange energies is difficult [Mur76] and established

expressions for these interactions are not available. Only recently, the role of these terms is becoming clear [LeS83, Lot97a, Buk01]. For example, Lotrich and Szalewicz [Lot97a], using fully *ab initio* three-body potentials containing short-range contributions calculated via a symmetry-adapted perturbation theory [Lot97b], computed the binding energy of solid argon. They found that the fcc crystal is favoured over the hcp crystal by 0.01%, in agreement with experimental observation.

Barker and Pompe [Bar68] in 1968 found a two-body potential for argon which, when used in conjunction with the AT potential, was able to reproduce the experimental crystal cohesive energy and third virial coefficient accurately. Even better agreement was found using the third-order *QQQ* and the forth-order *DDD* terms. Bobetic and Barker [Bob70], with the AT potential and a slightly different two-body potential, could reproduce the experimental data of specific heat, thermal expansion coefficient and the bulk modulus of crystalline argon. Barker et al. [Bar71a] using a combination of the previous potentials were able to reproduce gas, liquid and solid properties of argon with *Monte Carlo* and *molecular dynamics* simulations. Similar potentials were reported for krypton and xenon [Bar74]. Even if the pair + AT model was successful in reproducing experimental data, a theoretical justification for the exclusion of the three-body short-range terms was not given. A better evaluation and understanding of the many-body short-range potentials was necessary.

Other work followed to investigate this issue more deeply. Molecular beam scattering experiments on noble gases absorbed onto graphite substrate were performed to highlight the importance of short-range many-body effects. They could not provide a definitive solution, due to the lack of an accurate atom-substrate potential, but they showed the necessity of more accurate potentials [Azi89]. From a theoretical viewpoint, the first simultaneous implementation of the supermolecular Møller-Plesset perturbation

theory (MPPT) and intermolecular MPPT methods [Cha88] on Ar_3 showed that the second-order exchange effects were important for the total three-body effect near the potential minimum [Cha90].

A possible explanation of the contradiction between the success of the pair + AT model and the apparent importance of more recent work [Cha90] on the exchange effects can be provided by LeSar's crystal perturbation approach [LeS83]. LeSar used a 'crystal perturbation method' to obtain an approximate Hartree-Fock many-body interaction for the argon crystal. He found that the atomic orbitals in the crystal contract in comparison with those of the gas-phase atoms, resulting in less exchange repulsion. Equivalently in the gas-phase it can be thought that the higher-order exchange terms may cancel each other reducing the total short-range many-body effect significantly. McLean et al. [McL88] using the crystal perturbation many-body interaction + AT model for argon found excellent agreement with experimental solid state data.

Recently, Bukowsky and Szalewicz [Buk01] using symmetry-adapted perturbation theory potentials [Lot97b], performed simulations of liquid, gas and liquid-vapour equilibrium of argon. They found that even if three-body short-range contributions are large, cancellations occur at the interatomic distances typical for the liquid state, making the total three-body effect very similar to that given by the triple-dipole potential.

Experimental investigations

There are two main kinds of experiments to study the effects of many-body potentials: to the first kind belong those experiments that measure macroscopic properties, so they are sensitive just to the overall contribution of the many-body terms. Experiments of the second kind measure instead microscopic properties (mainly gas

phase interactions) and they are able to distinguish low-order terms in the many-body expansion.

The crystal structure of noble gases is evidence of the importance of the many-body potentials: X-ray diffraction reveals a face centered structure for the noble gases; instead the pair potentials predict a hexagonal close-packed structure (helium excluded). The inclusion of three-body terms in the potential provides a better agreement. Crystal cohesive energy measurements [Elr94] showed a 10% deviation from the pair potential prediction, suggesting again the presence of many-body effects. Crystal spacings, as well, provide information on repulsive and attractive contributions of many-body potentials.

Measurements of the radial distribution function of liquids with X-ray and neutron-scattering techniques [Ege88] give important indications, but they are not accurate enough to discriminate many-body effects. A recent detection of three-body effects was performed by Formisano et al. [For98] measuring the static structure factor $S(k)$ for xenon. The authors claimed to have obtained the first direct experimental determination of the triple-dipole Axilrod-Teller interaction. Many-body induced dipole moments and polarizability tensors can cause absorption and scattering of light in noble gases [Gui89a, Gui89b], while the two-body induced moment is exactly zero. Measurements of this kind of absorption spectrum can indicate many-body effects. It is more difficult to discern many-body effects from two-body ones using properties like viscosity, thermal conductivity and diffusion in gases.

So far we have briefly described experiments belonging to the first kind. Now we can examine those experiments measuring microscopic properties. The third virial coefficient, C in Eq. (2.8), depends on both two-and three-body potentials. Given a two-

body potential, u_2 , the contribution from the three-body terms, u_3 , is proportional to [Bar76]:

$$\Delta C \propto \iint e^{\left(\frac{u_2(r_{12})+u_2(r_{13})+u_2(r_{23})}{kT}\right)} \left\{ e^{\left(\frac{u_3(r_{12},r_{13},r_{23})}{kT}\right)} - 1 \right\} d\mathbf{r}_{12} d\mathbf{r}_{13} \quad (2.15)$$

where r_{ab} is the distance between atom **a** and **b**, whereas \mathbf{r}_{ab} is the corresponding vector. It was shown [Bar68] that ΔC contributes up to 50% of the value of the experimental C for noble gases.

The spectroscopy of van der Waals molecules provides a useful insight into the study of many body interactions. Recent high-resolution techniques have been used to measure intramolecular vibrational modes, which give direct information on the pair and higher order potentials [Elr94].

Theoretical techniques

From a theoretical viewpoint there are two complementary approaches to study the many-body effects: quantum mechanics and statistical mechanics. The latter consists mainly of *molecular dynamics* and *Monte Carlo* methods [All87]. As discussed later, modern developments in computer resources means that these methods can be used to investigate many-body potentials extensively.

Axilrod and Teller [Axi43, Axi51] were the first to use quantum mechanics calculations to find an analytic expression of a three-body potential. Nowadays there are two general methods used in *ab initio* techniques of weakly interacting systems: supermolecular and perturbation theory [Cha88]. In the supermolecular approach, the interaction energy between two systems is the difference between the energy of the complex and the monomers' energy. Perturbation theory considers the infinitely

separated monomers as the zero-order term, and the interaction energy comes from higher-order perturbations. This method provided the most important theoretical information about many-body interactions. Another relevant theoretical method is the Gaussian effective-electron model [Jan62] in which the exchange effects are approximated by placing on each atom one "effective" electron, with a Gaussian charge distribution.

A recent development of the perturbation theory technique is a simultaneous implementation of the supermolecular MPPT and intermolecular MPPT [Cha88]. This method allows the potential energy to be separated into exchange, electrostatic, induction and dispersion contributions [Szc92] as is generally done in the study of interaction forces. In this method the many-body induction (polarization) and exchange forces appear immediately in the perturbation expansion, while the many-body dispersion terms appear with each corresponding perturbation order. Another recent and promising technique is the mentioned symmetry-adapted perturbation theory [Lot97b].

Three-body dispersion potentials

Different types of interaction are possible depending on the distribution of multipole moments between the atoms. In principle, the dispersion, or long-range non-additive three-body interaction, is the sum of these various combinations of multipole moments [Bel70]. In this work, we have considered contributions from dipoles (D) and quadrupoles (Q) which are likely to make the most substantial effects on three-body dispersion:

$$u_{3bodyDisp} = u_{DDD} + u_{DDQ} + u_{DQQ} + u_{DDD4} + u_{QQQ} . \quad (2.16)$$

These terms are all third-order with the exception of the contribution of the fourth-order triple dipole term (u_{DDD4}). The main contribution to the three-body dispersion

interaction is the third-order triple-dipole term (u_{DDD}). The other terms collectively ($u_{DDQ} + u_{DQQ} + u_{QQQ} + u_{DDD4}$) are the higher multipole contributions.

The triple-dipole potential can be evaluated from the formula proposed by Axilrod and Teller [Axi43]:

$$u_{DDD} = \frac{v_{DDD} (1 + 3 \cos \mathbf{q}_i \cos \mathbf{q}_j \cos \mathbf{q}_k)}{(r_{ij} r_{ik} r_{jk})^3} \quad (2.17)$$

where the angles and intermolecular separations refer to a triangular configuration of atoms (see Figure 2.1) and where v_{DDD} is the non-additive coefficient which can be estimated from observed oscillator strengths [Leo75].

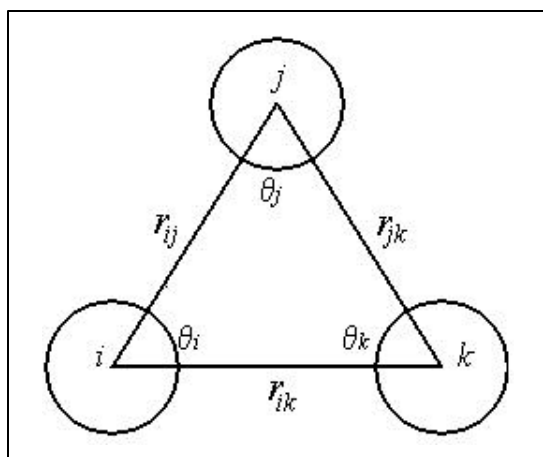


Figure 2.1 Triplet configuration of atoms i, j and k .

The contribution of the AT potential can be either negative or positive depending on the orientation adopted by the three atoms. The potential is positive for an acute triangular arrangement of atoms whereas it is negative for near linear geometries. The potential can be expected to make an overall repulsive contribution in a close-packed solid and in the liquid phase. The r^{-3} terms indicate that the magnitude of the potential is very sensitive to intermolecular separation.

Bell [Bel70] has derived the other multipolar non-additive third-order potentials:

$$u_{DDQ} = \frac{3v_{DDQ}}{16r_{ij}^3(r_{jk}r_{ik})^4} \times \left[9 \cos \mathbf{q}_k - 25 \cos 3\mathbf{q}_k + 6 \cos(\mathbf{q}_i - \mathbf{q}_j)(3 + 5 \cos 2\mathbf{q}_k) \right] \quad (2.18)$$

$$u_{DQQ} = \frac{15v_{DQQ}}{64r_{jk}^5(r_{ij}r_{ik})^4} \times \left[\begin{aligned} &3(\cos \mathbf{q}_i + 5 \cos 3\mathbf{q}_i) + 20 \cos(\mathbf{q}_j - \mathbf{q}_k)(1 - 3 \cos 2\mathbf{q}_i) \\ &+ 70 \cos 2(\mathbf{q}_j - \mathbf{q}_k) \cos \mathbf{q}_i \end{aligned} \right] \quad (2.19)$$

$$u_{QQQ} = \frac{15v_{QQQ}}{128(r_{ij}r_{ik}r_{jk})^5} \times \left[\begin{aligned} &-27 + 220 \cos \mathbf{q}_i \cos \mathbf{q}_j \cos \mathbf{q}_k + 490 \cos 2\mathbf{q}_i \cos 2\mathbf{q}_j \cos 2\mathbf{q}_k \\ &+ 175 [\cos 2(\mathbf{q}_i - \mathbf{q}_j) + \cos 2(\mathbf{q}_j - \mathbf{q}_k) + \cos 2(\mathbf{q}_k - \mathbf{q}_i)] \end{aligned} \right] \quad (2.20)$$

where Eqs (2.18), (2.19) and (2.20) represent the effect of dipole-dipole-quadrupole, dipole-quadrupole-quadrupole and quadrupole-quadrupole-quadrupole interactions, respectively. Formulae for the different ordering of the multipole moments on the three atoms (i.e., QDD , DQD , QDQ and QQD) can be generated from Eqs. (2.18) and (2.19) by cyclic permutation of the indices i , j and k . The dipole-dipole-octupole term has also been evaluated by Doran and Zucker [Dor71] but it is not considered in this work because of uncertainties in evaluating the DDO coefficient. The fourth-order triple-dipole term can be evaluated from [Dor71]:

$$u_{DDD4} = \frac{45v_{DDD4}}{64} \left[\frac{1 + \cos^2 \mathbf{q}_i}{(r_{ik}r_{ij})^6} + \frac{1 + \cos^2 \mathbf{q}_j}{(r_{ij}r_{jk})^6} + \frac{1 + \cos^2 \mathbf{q}_k}{(r_{ik}r_{jk})^6} \right]. \quad (2.21)$$

The coefficients for these three-body terms are summarised in Table 2.4.

Table 2.4 Coefficients for the three-body potentials in Eqs. (2.17), (2.18), (2.19), (2.20) and (2.21)

	argon	krypton	xenon
\mathbf{n}_{DDI} (a.u.) ^a	517.4	1554	5603
\mathbf{n}_{DDQ} (a.u.) ^b	687.5	2272	9448
\mathbf{n}_{DQQ} (a.u.) ^b	2687	9648	45770
\mathbf{n}_{QQQ} (a.u.) ^b	10639	41478	222049
\mathbf{n}_{DDD4} (a.u.) ^c	-10570	-48465	-284560

^a from ref. [Leo75]

^b from ref. [van98]

^c from ref. [Bad58]

Strategies for calculating multipole moments have been discussed recently [van98]. Combining the contributions from two-body and three body interactions yields an overall intermolecular potential for the fluid:

$$u(r) = u_2(r) + u_{3bodyDisp}(r). \quad (2.22)$$

Table 2.5 displays the contributions to the internal energy and pressure of liquid argon that Barker et al. [Bar71a] calculated with Monte Carlo simulations using the pair + AT model, compared with the relevant experimental quantities.

Table 2.5 Contributions to the internal energy and to the pressure of liquid argon [Bar71a].

T (K)	V (cm^3/mol)	$E^{(a)}$ (cal/mol)	E^{3-body} (cal/mol)	$E^{Quant.}$ (cal/mol)	$E^{Tot.}$ (cal/mol)	$E^{Exp.}$ (cal/mol)	$P^{(a)}$ (atm)	P^{3-body} (atm)	$P^{Quant.}$ (atm)	$P^{Tot.}$ (atm)	$P^{Exp.}$ (atm)
100.00	27.04	-1525.2	87.1	15.6	-1423	-1432	239.9	364.2	42.2	646	652
100.00	29.66	-1393.6	67.9	12.5	-1313	-1324	-148.0	238.8	25.3	116	105
140.00	30.65	-1284.7	62.8	9.3	-1213	-1209	348.9	214.3	16.7	580	583
140.00	41.79	-951.4	39.5	6.4	-906	-922	-33.7	49.0	2.7	18	37
150.87	70.73	-603.8	26.6	4.6	-573	-591	34.5	13.2	1.2	49	49

^(a)kinetic part + 2-body potential part

As shown in Table 2.5 the agreement with experiment is very good. Just the pressure at $T = 140$ K and $V = 41.79$ cm^3/mol diverges significantly from the experimental value. It is particularly noteworthy that the three-body contribution for the pressure plays a fundamental role to match the experimental results. For both energy and pressure, however, the quantum contribution is of minor importance.

As for argon, Barker et al. [Bar74], in using condensed phase data to derive two-body potentials for krypton and xenon in Eq. (2.12), considered three-body interactions as well. For krypton the Axilrod-Teller potential is the most relevant 3-body interaction, since the third-order dipole-quadrupole and the forth-order triple-dipole interactions

roughly cancel each other. For xenon instead, this cancellation is not complete, so Barker et al. [Bar74] considered the latter contributions deriving the two-body potential.

2.2 Monte Carlo simulation of phase equilibria

Here we give details of a molecular simulation technique, Gibbs ensemble [Pan88], which allows one to study coexisting phases of fluids. We used this technique to simulate the noble gas vapour-liquid phase. Molecular simulation is a complementary tool to the experiments and theory used to investigate the properties of thermodynamic systems and phase behavior of fluids. The latter task is not an easy one from a computational viewpoint. Phase transitions are collective phenomena that occur over long time and length scales that are difficult to reproduce by traditional molecular simulation techniques [All87]. In a system at liquid-vapour equilibria, the interface between the two phases has a prominent influence on the bulk properties if the number of particles used in the simulation is small. Hence, a large number of particles is required to avoid this problem. New simulation techniques are now available [Pan00] and amongst them the Gibbs ensemble is outstanding for its simplicity and predictive power. It eliminates the problem of the interface, performing the simulation in two different boxes, each of which contains one of the two phases considered. Even if they are separate, the boxes are correlated through particle exchanges and volume fluctuation. This characteristic permits simulations of phase equilibria utilizing a reasonable number of particles.

In section 2.2.1 we give some details of the Metropolis method, which is largely used in the Monte Carlo techniques [All87]. In section 2.2.2 we introduce the Gibbs ensemble technique, discussing the theoretical foundations and how to implement it.

2.2.1 Metropolis method

Monte Carlo simulations may be used to study molecular systems utilizing statistical mechanics. Considering for simplicity a *canonical* ensemble at temperature T , with N particles and a hamiltonian $H(\mathbf{r}^N, \mathbf{p}^N)$, where \mathbf{r}^N and \mathbf{p}^N are positions and momenta of the particles respectively, the average value of any quantity $A(\mathbf{r}^N, \mathbf{p}^N)$ is given by [Fre96]:

$$\langle A \rangle = \frac{\int d\mathbf{p}^N d\mathbf{r}^N A(\mathbf{r}^N, \mathbf{p}^N) \exp(-H(\mathbf{r}^N, \mathbf{p}^N)/kT)}{\int d\mathbf{p}^N d\mathbf{r}^N \exp(-H(\mathbf{r}^N, \mathbf{p}^N)/kT)} \quad (2.23)$$

where the integrals are calculated over the *phase space* of the system. Usually the hamiltonian has a quadratic dependence on the momenta and for any quantity $A(\mathbf{p}^N)$, depending just on the momenta, Eq. (2.23) is easy to calculate. More difficult is the evaluation of the average value of quantities $A(\mathbf{r}^N)$. In this case Eq. (2.23) becomes:

$$\langle A \rangle = \frac{\int d\mathbf{r}^N A(\mathbf{r}^N) \exp(-u(\mathbf{r}^N)/kT)}{\int d\mathbf{r}^N \exp(-u(\mathbf{r}^N)/kT)} . \quad (2.24)$$

There are different techniques to calculate Eq. (2.24). A naive method is to generate a number of random configurations (\mathbf{r}^N) of the particles, calculate the relative values of $A(\mathbf{r}^N)$ and energy $u(\mathbf{r}^N)$ and to give each configuration a weight according to the Boltzmann factor ($\exp(-u(\mathbf{r}^N)/kT)$). Unfortunately, for the majority of configurations the Boltzmann factor ($\exp(-u(\mathbf{r}^N)/kT)$) is vanishingly small. It is more convenient instead to use the Monte Carlo importance-sampling method introduced by Metropolis et al. [Met53].

The expression in Eq. (2.24)

$$P(\mathbf{r}^N) = \frac{\exp(-u(\mathbf{r}^N)/kT)}{\int d\mathbf{r}^N \exp(-u(\mathbf{r}^N)/kT)} \quad (2.25)$$

represents the probability density to find the system in a configuration around \mathbf{r}^N . The Metropolis method then consists in generating configurations according to the probability density $P(\mathbf{r}^N)$, in order to consider configurations which give relevant contributions to Eq. (2.24) and then weight them evenly. An initial configuration (*old*) is chosen with a non-vanishing Boltzmann factor ($\exp(-u_{old}/kT)$), usually positioning the atoms in crystalline lattice sites. A *new* configuration is generated, for example by adding a small displacement to the old position of an atoms; the relative Boltzmann factor ($\exp(-u_{new}/kT)$) is calculated. At this stage it has to be decided whether to accept or reject the new configuration. Namely a transition probability, $\mathbf{p}(old \rightarrow new)$, to go from configuration *old* to *new* has to be determined. This transition probability can be expressed as:

$$\mathbf{p}(old \rightarrow new) = \mathbf{a}(old \rightarrow new) \times acc(old \rightarrow new) \quad (2.26)$$

where $\mathbf{a}(old \rightarrow new)$ is a transition matrix (Markov chain matrix [All87, Hoh93]) that indicates the probability to perform a trial move from *old* to *new*, and where $acc(old \rightarrow new)$ is the probability of accepting a trial move from *old* to *new*. It is useful to point out here that the Metropolis method does not need to have any knowledge about the momenta of the particles, and the temperature of the system is chosen *a priori* as a parameter.

In the Metropolis method $\mathbf{a}(old \rightarrow new)$ is chosen to be a symmetric matrix, $\mathbf{a}(old \rightarrow new) = \mathbf{a}(new \rightarrow old)$ (even if non symmetric matrixes could be chosen [Fre96]), and it is assumed that at equilibrium the average number of accepted moves

from *old* to any other *new* state is exactly cancelled by the number of reverse moves.

The former is the detailed balanced condition that implies:

$$P(old)\mathbf{p}(old \rightarrow new) = P(new)\mathbf{p}(new \rightarrow old) \quad . \quad (2.27)$$

Since \mathbf{a} is symmetric, Eq. (2.27) can be written as:

$$P(old) \times acc(old \rightarrow new) = P(new) \times acc(new \rightarrow old) \quad (2.28)$$

or:

$$\frac{acc(old \rightarrow new)}{acc(new \rightarrow old)} = \frac{P(new)}{P(old)} = \exp\left(-\frac{(u_{new} - u_{old})}{kT}\right) \quad . \quad (2.29)$$

Eq. (2.29) can be satisfied with many different choices for $acc(old \rightarrow new)$. In the Metropolis method the following choice is used:

$$acc(old \rightarrow new) = \begin{cases} P(new)/P(old) & \text{if } P(new) < P(old) \\ 1 & \text{if } P(new) \geq P(old) \end{cases} \quad . \quad (2.30)$$

This means that if $P(new) \geq P(old)$, ($u_{new} \leq u_{old}$), the trial move has to be accepted, otherwise it has to be accepted with a probability $\frac{P(new)}{P(old)} = \exp\left(-\frac{(u_{new} - u_{old})}{kT}\right)$. In the latter case a random number, from a uniform distribution in the interval [0,1], is generated and if this number is less than $acc(old \rightarrow new)$ the trial move is accepted. It is important to stress that the only condition imposed on $\mathbf{a}(old \rightarrow new)$ is that it has to be symmetric. For this reason several trial moves can be chosen, according to the ensemble under study. The Metropolis method, in fact, can be used for any ensemble but obviously the acceptance criteria depends on the partition function of the ensemble considered. Importantly, any choice of the trial moves has to satisfy the ergodic condition, namely that every point in configuration space can be reached in a finite number of Monte Carlo steps from any other point.

In the following sections the trial moves used in the Gibbs ensemble technique and the relative acceptance criteria are given.

2.2.2 Gibbs ensemble technique

The condition for achieving coexistence of two or more phases I, II, \dots at equilibrium is that the pressure and temperature in each phase must be equal ($P_I = P_{II} = \dots = P$; $T_I = T_{II} = \dots = T$), as do the chemical potentials of all the species ($\mu_I^a = \mu_{II}^a = \dots = \mu^a$). Unfortunately, it is impossible to study such systems with an ensemble where pressure, temperature and chemical potentials are fixed, since they are linearly dependent quantities, or equivalently, because constraining only intensive quantities like pressure, temperature and chemical potentials leaves the extensive quantities unbounded [Fre96].

The Gibbs ensemble technique [Pan87, Pan88] is able to study phase equilibria under the conditions that the pressure, temperature and chemical potential of the coexisting phases are equal. This is possible because even if the difference between the chemical potentials in different phases is fixed ($\Delta\mu = 0$) the absolute values are undetermined. We applied the Gibbs ensemble technique to simulate noble gas vapour-liquid phase equilibria.

Theoretical foundations of the NVT Gibbs ensemble

The Gibbs ensemble Monte Carlo technique is used to simulate phase equilibria in fluids. To reproduce a macroscopic system with two coexisting phases in equilibrium, the Gibbs ensemble method simulates two separate microscopic regions within the bulk phases, away from the interface. Standard periodic boundary conditions, namely the

minimum image convention [All87], are applied. Three types of Monte Carlo moves are performed: displacements of particles within each region to satisfy internal equilibrium; fluctuations in the volume of the regions to achieve equality of the pressure; and exchanges of particles between regions to achieve equality of chemical potentials of all the species. Figure 2.2 depicts the three different moves.

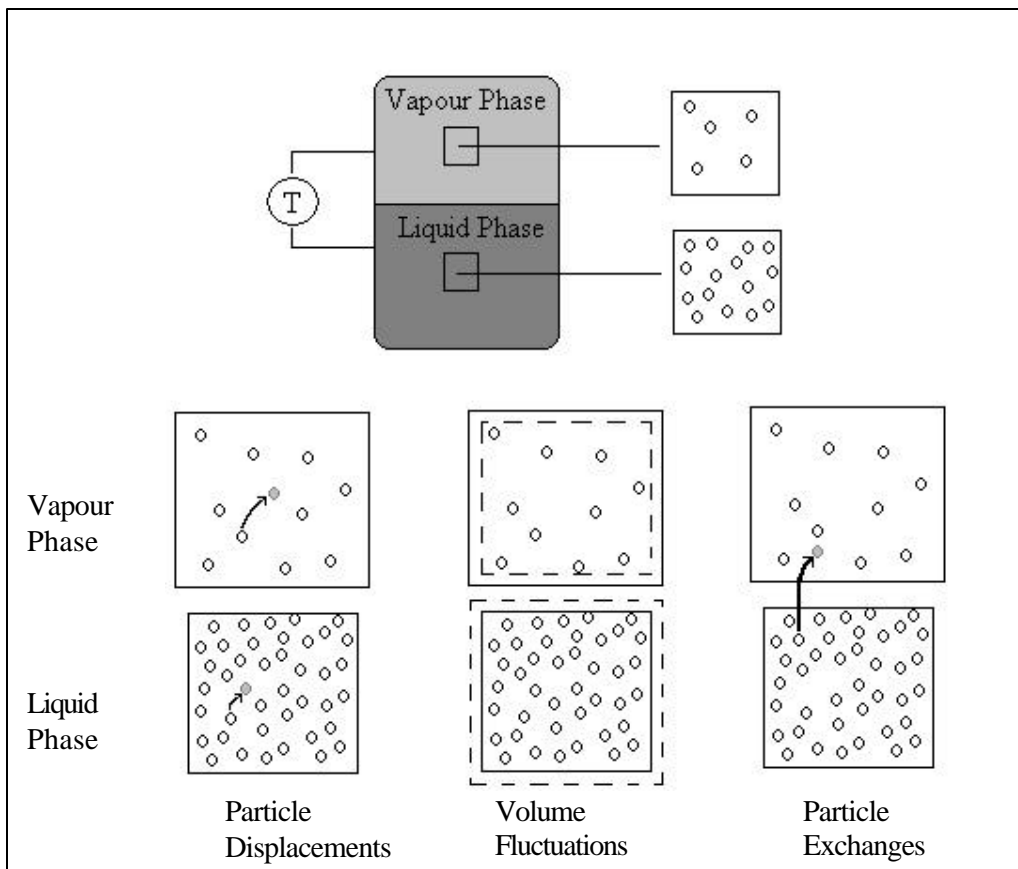


Figure 2.2 Representation of the Gibbs ensemble Monte Carlo simulation methodology.

Panagiotopoulos [Pan87] first derived the acceptance criterion from fluctuation theory, making an approximation for the particle exchange which led to a difference proportional to $1/N$, relative to the exact expression given later [Pan88]. A rigorous statistical mechanics derivation of the ensemble was reported by Smit et al. [Smi89a] and by Smit and Frenkel [Smi89b].

We are interested in the version of the Gibbs ensemble where the temperature (T), the total number of particles ($N = n_I + n_{II}$) and the total volume ($V = V_I + V_{II}$) of the two regions (boxes), I and II , are fixed. The partition function counts the number of possibilities in which N particles can be distributed in those two boxes with variable volumes, and can be expressed as [Pan95]:

$$Q_{NVT} = \frac{1}{\Lambda^{3N} N!} \sum_{n_I=0}^N \frac{N!}{n_I! n_{II}!} \int_0^V dV_I V_I^{n_I} V_{II}^{n_{II}} \int d\mathbf{x}_I^{n_I} \exp(-u(\mathbf{x}_I^{n_I})/kT) \times \int d\mathbf{x}_{II}^{n_{II}} \exp(-u(\mathbf{x}_{II}^{n_{II}})/kT) \quad (2.31)$$

where \mathbf{x} are the scaled coordinates of the particles in two boxes, $u(\mathbf{x}_I^{n_I})$ and $u(\mathbf{x}_{II}^{n_{II}})$ are the total potential energies in each box (depending on the intermolecular potential used) and Λ is the thermal de Broglie wavelength ($\Lambda = \sqrt{h^2/(2pmk_B T)}$). It can be demonstrated that the constant-volume Gibbs ensemble in the thermodynamic limit is equivalent to the canonical ensemble [Smi89a].

Eq. (2.31) states that the probability of finding the system with n_I particles in box I (with volume V_I) and positions $\mathbf{x}_I^{n_I}$ and the rest of the particles in positions $\mathbf{x}_{II}^{N-n_I}$, is given by:

$$P(n_I, V_I, \mathbf{x}_I^{n_I}, \mathbf{x}_{II}^{N-n_I}) \propto \frac{N! V_I^{n_I} (V_{II})^{N-n_I}}{n_I! (N-n_I)!} \exp\{-[u(\mathbf{x}_I^{n_I}) + u(\mathbf{x}_{II}^{N-n_I})]/kT\}. \quad (2.32)$$

Using Eq. (2.32) and the detailed balance condition (Eq. (2.27)) it is possible to derive the acceptance rules [Pan88, Fre96] for trial moves for the Gibbs ensemble simulations.

For the particle displacement, the *new* configuration is generated from the *old* one, displacing randomly a particle in box I . The ratio between the probability relative to the *new* configuration and the probability relative to the *old* configuration is given by:

$$\frac{P(new)}{P(old)} = \frac{\exp\{-[u(\mathbf{x}_{I-new}^{n_I})]/kT\}}{\exp\{-[u(\mathbf{x}_{I-old}^{n_I})]/kT\}} \quad (2.33)$$

Substituting Eq. (2.33) in Eq. (2.29) allows one to derive the probability of accepting the *new* configuration:

$$acc(old \rightarrow new) = \min(1; \exp\{-[u(\mathbf{x}_{I-new}^{n_I}) - u(\mathbf{x}_{I-old}^{n_I})]/kT\}) \quad (2.34)$$

In general, if the move is rejected, the *old* configuration is kept.

For the volume fluctuation, the box to be expanded is randomly chosen. If the chosen box (say box *I*) is expanded by ΔV ($V_{new}^I = V_{old}^I + \Delta V$) the other is compressed by ΔV ($V_{new}^{II} = V_{old}^{II} - \Delta V$), in order to keep the total volume constant. Using eq (2.32), the ratio between the probability relative to the *new* configuration and the probability relative to the *old* configuration can be expressed as:

$$\frac{P(new)}{P(old)} = \frac{(V_{new}^I)^{n_I} (V_{new}^{II})^{N-n_I} \exp\{-[u(\mathbf{x}_{new}^N)]/kT\}}{(V_{old}^I)^{n_I} (V_{old}^{II})^{N-n_I} \exp\{-[u(\mathbf{x}_{old}^N)]/kT\}} \quad (2.35)$$

and the probability of accepting the *new* configuration is given by:

$$acc(old \rightarrow new) = \min \left(1; \frac{(V_{new}^I)^{n_I} (V_{new}^{II})^{N-n_I} \exp\{-[u(\mathbf{x}_{new}^N)]/kT\}}{(V_{old}^I)^{n_I} (V_{old}^{II})^{N-n_I} \exp\{-[u(\mathbf{x}_{old}^N)]/kT\}} \right) \quad (2.36)$$

In writing Eq. (2.36) we assumed that the Markov chains sampled by each box are not effected by the perfectly correlated volumes. This is a good approximation away from the critical point [Pan88].

For the particle exchange one of the two boxes is randomly chosen (say box *I*). One particle is removed from the box and inserted into the other box randomly choosing the new coordinates. The ratio between the probability relative to the *new* configuration and the probability relative to the *old* configuration can be expressed as:

$$\frac{P(new)}{P(old)} = \frac{n_I!(N-n_I)!(V^I)^{n_I-1}(V-V^I)^{N-(n_I-1)} \exp\{-[u(\mathbf{x}_{new}^N)]/kT\}}{(n_I-1)!(N-(n_I-1))!(V^I)^{n_I}(V-V^I)^{N-n_I} \exp\{-[u(\mathbf{x}_{old}^N)]/kT\}} \quad (2.37)$$

and the probability of accepting the *new* configuration is given by:

$$acc(old \rightarrow new) = \min \left(1; \frac{n_I(V-V^I) \exp\{-[u(\mathbf{x}_{new}^N)]/kT\}}{(N-n_I+1)V^I \exp\{-[u(\mathbf{x}_{old}^N)]/kT\}} \right). \quad (2.38)$$

Implementation

The method we used to generate trial configurations is the original implementation [Pan88] where the different trial moves are performed in a fixed order. The simulation is carried in cycles. Each cycle consists of N displacements to move all the particles in each box, one attempt to change the volume and N attempts to exchange all the particles. We chose, as the initial configuration of each simulation, a face-centred cubic lattice with the desired number of particles in each box positioned randomly. A number of cycles were carried out to reach equilibrium; after this phase the macroscopic physical quantities are accumulated.

For the particle displacement moves, the *old* coordinates of the randomly selected particle (more precisely its center of mass) are changed adding random numbers between $-\Delta_{\max}$ and Δ_{\max} , where Δ_{\max} is the maximum displacement allowed:

$$\begin{aligned} x_{new} &\leftarrow x_{old} + (2 \times rand - 1) \times \Delta_{\max} \\ y_{new} &\leftarrow y_{old} + (2 \times rand - 1) \times \Delta_{\max} \\ z_{new} &\leftarrow z_{old} + (2 \times rand - 1) \times \Delta_{\max} \end{aligned} \quad (2.39)$$

rand is a random number from a uniform distribution in the interval [0,1]. We chose Δ_{\max} in order to have at least 50% acceptance rate. The 50% acceptance rate has no theoretical basis. Mountain and Thirumalai discussed criteria for determining the efficiency of the particle displacement moves [Mou94]. The potential energies with the

particle in the *old* position and in the new position respectively are calculated and the acceptance criterion (Eq. (2.34)) applied. It is noteworthy to stress that Eq. (2.34) requires the difference between the potential energies relative to the two configurations, so only the intermolecular energy relative to the displaced particle and the rest of the particles are required.

For the volume fluctuation move, one box, chosen randomly, is expanded by ΔV and the other compressed by $-\Delta V$. The quantity ΔV is given by:

$$\Delta V = \mathbf{z} \times \Delta V_{\max} \times \min(V^I; V^II) \quad (2.40)$$

where \mathbf{z} is a uniformly distributed random number in the range [0,1] and ΔV_{\max} is the maximum fractional volume change allowed. Typically, ΔV_{\max} is chosen in order to have at least 50% acceptance rate, which should guarantee that equilibrium is achieved efficiently. However, this does not have any theoretical justification. The following quantities are calculated:

$$Rat^i = \sqrt[3]{\frac{V_{new}^i}{V_{old}^i}} \quad i = I, II \quad (2.41)$$

and used to scale the coordinates of the particles in each box:

$$\begin{aligned} x_{new}^i &\leftarrow x_{old}^i \times Rat^i \\ y_{new}^i &\leftarrow y_{old}^i \times Rat^i \\ z_{new}^i &\leftarrow z_{old}^i \times Rat^i \end{aligned} \quad i = I, II \quad (2.42)$$

The potential energies relative to the *old* and *new* coordinates are calculated and the acceptance criterion (Eq. (2.36)) applied.

For the exchange particle move, a randomly selected particle is ‘cancelled’ from its original box and inserted into the other. The *new* coordinates of the particle are randomly assigned in the following way (the centre of the simulation box is the origin of the coordinates):

$$\begin{aligned}
x_{new} &\leftarrow (rand - 0.5) \times L \\
y_{new} &\leftarrow (rand - 0.5) \times L \quad L = \text{Box length} \quad . \\
z_{new} &\leftarrow (rand - 0.5) \times L
\end{aligned} \tag{2.43}$$

As with the particle displacement, in order to apply the acceptance criterion in the exchange move (Eq. (2.38)) only the potential energy between the exchanged particle and the rest of the particles is required. For the exchange particle moves, in our simulations we had at least 20% acceptance rate.

***NPT* ensemble for binary mixtures**

A constant pressure Gibbs ensemble [Pan88] can be performed only with mixtures, since for pure components the two-phase region is a line in the P - T plane. Thus any choice of P and T corresponds to a vanishingly small probability that the system is at the phase transition. For two-component systems the two-phase region is a finite area in the P - T plane [Fre96].

In the case of a NPT ensemble for binary mixtures, total number of particles, pressure and temperature are kept constant. The total number of particles is the sum of the total number of particles of both species, a and b , ($N = N^a + N^b$). The acceptance criterion for the particle displacement is the same as in Eq. (2.34). In the particle exchange acceptance criterion (Eq. (2.38)) n_I and $n_{II} = N - n_I$ now represent the number of particles of the species, for example a , being exchanged, (n_I^a and $n_{II}^a = N^a - n_I^a$) [Pan88]. The volume fluctuation acceptance criterion (Eq. (2.36)) becomes [Pan88]:

$$acc(old \rightarrow new) = \min \left(1; \frac{(V_{new}^I)^{n_I^a + n_I^b} (V_{new}^{II})^{n_{II}^a + n_{II}^b} \exp\{-[u(\mathbf{x}_{new}^N) + P(\Delta V^I + \Delta V^{II})]/kT\}}{(V_{old}^I)^{n_I^a + n_I^b} (V_{old}^{II})^{n_{II}^a + n_{II}^b} \exp\{-[u(\mathbf{x}_{old}^N)]/kT\}} \right) \tag{2.44}$$

where in this case it is possible that $\Delta V^I \neq -\Delta V^{II}$ since the total volume is not constant.

Calculation of the chemical potential

One of the requirements for phase equilibrium is the equality of the chemical potential (material equilibrium). A common technique used to calculate the chemical potential is the Widom test particle method [Wid63], which utilizes the interaction energy of a ‘ghost’ particle inserted into the system. The Gibbs ensemble technique does not rely on the knowledge of the chemical potential, but its calculation during the simulation can provide a useful check to ensure that equilibrium is achieved. During an exchange trial the energy of the particle inserted corresponds to the energy of a ‘ghost’ particle, so it is possible to calculate the chemical potential with ease.

Following the procedure reported by Smit et al. [Smi89b], the chemical potential is given by:

$$\mathbf{m} = -kT \ln \left(\frac{Q_{N+1}}{Q_N} \right) \quad (2.45)$$

where Q_N is the partition function (here we use the Gibbs ensemble Q_N , eq (2.31), at constant (N, V, T)). Substituting Eq. (2.31) in Eq. (2.45) and assuming that the boxes do not change ‘identity’ during the simulation, the expressions for the chemical potentials in both phases are:

$$\begin{aligned} \mathbf{m}_I &= -kT \ln \frac{1}{\Lambda^3} \left\langle \frac{V_I}{n_I + 1} \exp(-\Delta u_I^+) \right\rangle_I \\ \mathbf{m}_{II} &= -kT \ln \frac{1}{\Lambda^3} \left\langle \frac{V_{II}}{n_{II} + 1} \exp(-\Delta u_{II}^+) \right\rangle_{II} \end{aligned} \quad (2.46)$$

where $\langle \rangle_I$ represents an ensemble average in the Gibbs ensemble restricted to box I and Δu_I^+ is the energy of a ‘ghost’ particle in box I (equivalently for $\langle \rangle_{II}$ and Δu_{II}^+).

Finite-size effects at criticality

In general, phase transitions consist of changes between an ordered state and a disordered state. Thermodynamic properties of systems approaching the transition point can show anomalies due to complex microscopic behaviour which gives rise to observable macroscopic effects. As the disordered region of the transition approaches the ordered one, individual microscopic fluctuations start to have a strongly correlated behavior. Close to the transition, the size of the region over which this coherence extends becomes so large that it persists out to macroscopic lengths.

In the Gibbs ensemble technique the use of a finite system and periodic boundary conditions makes the study of phase transitions close to the critical points difficult. In a real system the correlation length that measures the spatial extent of density fluctuations tend to infinity. The finite size simulation cell can not capture this behaviour. Work regarding the finite-size effects on the Gibbs ensemble was reported [Rec93, Pan94b] in two- and three-dimension, for symmetric square-well and Lennard-Jones fluids.

In the Gibbs ensemble, away from the critical region of the phase transition, the densities and compositions of both phases can be evaluated by averaging these quantities in each simulation box. When approaching the critical point, anomalous fluctuations in the density and composition are observed, due to the formation of droplets or bubbles of the opposite phase in one of the two boxes. Under these conditions, a procedure of collecting information is to use histograms of the frequency of occurrence of a certain density in each of the two boxes. The equilibrium densities can be defined as the densities relative to the peaks of the probability distribution function [Pan95]. Getting even closer to the critical point, the free energy penalty for formation of interfaces in both boxes becomes smaller [Sm89a] and exchanges of

identities of the two boxes are observed. The coexisting densities can not be determined with high accuracy [Pan95].

To predict the critical temperature and density using the Gibbs ensemble simulations the rectilinear diameter rule and scaling relationship are applied [Pan95]:

$$\frac{\mathbf{r}_{liq} - \mathbf{r}_{vap.}}{2} = \mathbf{r}_{crit} + C(T_{crit.} - T); \quad \mathbf{r}_{liq.} - \mathbf{r}_{vap.} \propto (T_{crit.} - T)^b \quad (2.47)$$

where \mathbf{b} is an exponent that experimental results and modern theories of critical phenomena indicate to be ≈ 0.325 in three-dimension [Pan95]. It was shown that for Lennard-Jones fluids [Pan94b] the use of Eq. (2.47) predicts the critical temperature within an accuracy of $\pm 1\%$, but it gives a significantly larger uncertainty for the critical density.

At this stage we point out that it is not the interest of our work to determine critical temperature and density of the systems simulated, since our aim is only to test the interatomic potentials for coexisting phases.

Some mathematical considerations

The NVT Gibbs ensemble is characterized by a simple mathematical constraint that, to our knowledge, has never been highlighted. The only reference found to this issue is reported by Bruce [Bru97] which we quote to introduce the issue itself:

“In Gibbs ensemble one needs only to ensure that the overall density lies somewhere in the range between those of the coexisting phases; this constraint sharpens with the approach to the critical point” [Bru97].

Considering the one species case we can write the system of equations:

$$N = N_I + N_{II}; \quad V = V_I + V_{II}; \quad \mathbf{r}_I = \frac{N_I}{V_I}; \quad \mathbf{r}_{II} = \frac{N_{II}}{V_{II}} \quad (2.48)$$

where N_I (N_{II}), V_I (V_{II}) and \mathbf{r}_I (\mathbf{r}_{II}) are the number of particles, the volume and density at any time in box I (II) respectively. For each simulation the total number of particles, N , the total volume, V , and consequently the total density ($\mathbf{r} = \frac{N}{V}$) are fixed.

The question we want to answer is:

given the total density $\mathbf{r} = \frac{N}{V}$, is it possible to accommodate any value of \mathbf{r}_I and \mathbf{r}_{II} in box I and II at any time during the simulation?

For this purpose we have to find the solutions for the variables (unknowns) N_I , N_{II} , V_I and V_{II} of the system in Eq. (2.48), where N and V are fixed values (chosen from the simulation) and \mathbf{r}_I and \mathbf{r}_{II} are any given positive values. Using simple methods of linear algebra one can show that, if

$$\mathbf{r}_I \neq \mathbf{r}_{II} \quad (2.49)$$

the system in Eq. (2.48) always has the solution:

$$N_I = \frac{N - \mathbf{r}_{II}V}{1 - \frac{\mathbf{r}_{II}}{\mathbf{r}_I}} ; V_I = \frac{N - \mathbf{r}_{II}V}{\mathbf{r}_I - \mathbf{r}_{II}} \quad (2.50)$$

but we have to impose that :

$$0 \leq N_I \leq N ; 0 \leq V_I \leq V \quad (2.51)$$

which are satisfied if:

$$\mathbf{r}_I \leq \mathbf{r} \leq \mathbf{r}_{II} \text{ or } \mathbf{r}_{II} \leq \mathbf{r} \leq \mathbf{r}_I . \quad (2.52)$$

So the answer to the above question is 'yes' as long as \mathbf{r}_I and \mathbf{r}_{II} satisfy Eq. (2.52). This means that during the simulation the density in one box is at any instant greater than or equal to \mathbf{r} while in the other box is less than or equal to \mathbf{r} , as physical intuition suggests. In order to obtain the expected results, \mathbf{r} must be chosen to lie

between the expected densities of the two coexisting phases, if they are known. If they are not known, explorative runs have to be performed. When \mathbf{r} is chosen outside the coexisting diagram the densities in both boxes happen to fluctuate near the value of \mathbf{r} . This is a clear signal that a different value of \mathbf{r} has to be chosen.

In the case of NPT Gibbs ensemble for binary mixture we have to follow the same scheme. The total number of particles of both species, N^a and N^b , are fixed. The question we want to answer now is:

given the total number of particles of both species, N^a and N^b , is it possible to accommodate in box I and II any value of \mathbf{r}_I and \mathbf{r}_{II} and any value of the compositions (x_I^a, x_I^b, x_{II}^a and x_{II}^b) at any time during the simulation?

The system of equations we now have to consider is:

$$\left. \begin{aligned} N^a &= N_I^a + N_{II}^a ; N^b = N_I^b + N_{II}^b \\ \mathbf{r}_I &= \frac{N_I^a + N_I^b}{V_I} ; \mathbf{r}_{II} = \frac{N^a - N_I^a + N^b - N_I^b}{V_{II}} \\ x_I^a &= \frac{N_I^a}{N_I^a + N_I^b} ; x_{II}^a = \frac{N^a - N_I^a}{N^a - N_I^a + N^b - N_I^b} \end{aligned} \right\} \quad (2.53)$$

where the unknowns are $V_I, V_{II}, N_I^a, N_{II}^a, N_I^b$ and N_{II}^b and the conditions to impose are:

$$0 \leq N_I^a \leq N^a \quad (2.54)$$

$$0 \leq N_I^b \leq N^b \quad (2.55)$$

which are satisfied if:

$$\frac{x_{II}^a}{x_{II}^b} \leq \frac{N^a}{N^b} \leq \frac{x_I^a}{x_I^b} \quad \text{for } x_I^a \geq x_{II}^a \quad (2.56)$$

or equivalently:

$$\frac{x_{II}^a}{1-x_{II}^a} \leq \frac{N^a}{N-N^a} \leq \frac{x_I^a}{1-x_I^a} \quad \text{for } x_I^a \geq x_{II}^a \quad . \quad (2.57)$$

Again, the answer to the above question is ‘yes’ as long as N^a and N^b satisfy Eqs. (2.56) or (2.57). Eqs. (2.56) and (2.57) state that the ratio N^a / N^b should not to be chosen greater (or less) than both x_{II}^a / x_{II}^b and x_I^a / x_I^b , as physical intuition suggests. For a NPT Gibbs ensemble with more than two components the answer to the above question is in general negative. This is because the equivalent system to Eq. (2.53), for example in a three-component mixture case, would contain 9 equations in 8 unknowns, which is in general not solvable. This does not mean that the simulation is not feasible. In fact, in the Gibbs ensemble technique the average values of the compositions and densities are important and not just the instantaneous values. However, Eq. (2.57) *must* be satisfied for each component. Similar considerations apply for a multicomponent NVT Gibbs ensemble, in which Eqs. (2.52) and (2.57) *must* be satisfied.

2.3 Synthetic Non-Equilibrium Molecular Dynamics

In this section we focus on planar Couette flow where adjacent parts of the fluid are moving with different relative velocities. Such systems are not in thermodynamic equilibrium, so viscous forces generate the transport of momentum between co-moving layers. A non-equilibrium molecular dynamics computer simulation [All87, Eva90] allows one to solve the equations of motion of each molecule of the system, and directly calculate the transport coefficients. In the following sections we describe the computer technique known as synthetic non-equilibrium molecular dynamics (NEMD) [Eva90] applied to planar Couette flow, which is used to calculate the shear viscosity of the fluid directly from the dynamics of the system (see Chapter 4).

In section 2.3.1 we give some details of homogeneous planar Couette flow, introducing the physical quantities necessary to describe the transport of momentum, namely the pressure tensor, strain rate and shear viscosity. In section 2.3.2 we describe how to derive these quantities from a microscopic description. In section 2.3.3 we give some details of the NEMD algorithm to simulate planar Couette flow, and in the last section we introduce the non-equilibrium pair distribution function which provides insight into the structure of the fluid and allows one to calculate the pressure, energy and viscosity indirectly.

2.3.1 Planar Couette flow

Figure 2.3 depicts a planar Couette flow where an atomic fluid is confined by two parallel plates of area A , distant L apart.

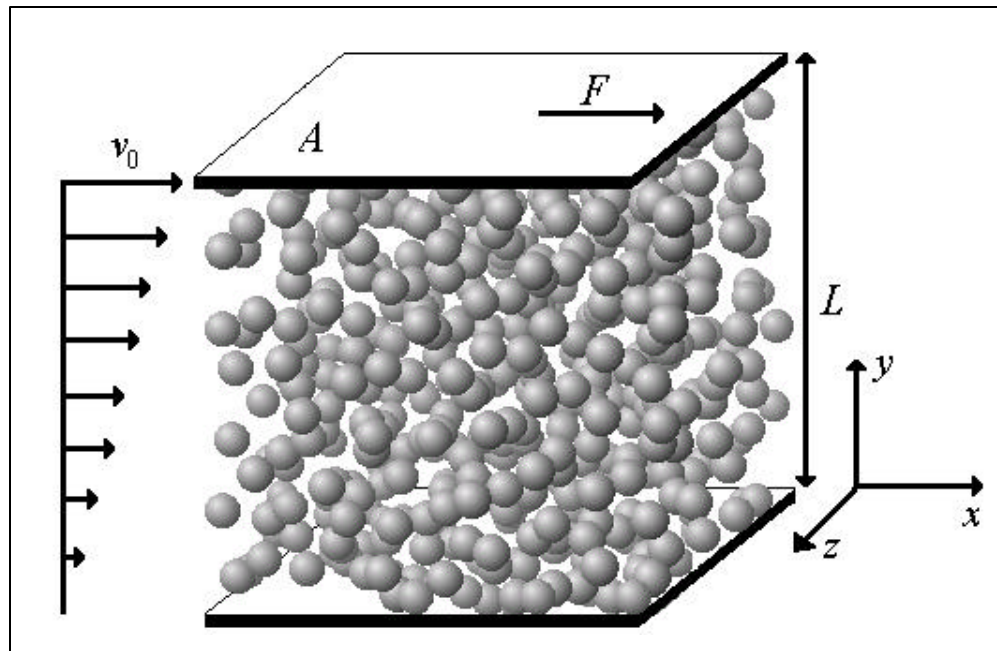


Figure 2.3 Laminar flow of an atomic fluid between a moving upper plate and stationary lower plate.

The upper plate slides in the positive x -direction at a constant velocity v_0 , while the other plate is stationary. Here L is a macroscopic quantity, or more precisely, L is much larger than the range of the interatomic interactions.

Two general types of behaviour can occur depending on the nature of the fluid. With some fluids the force F used to maintain the velocity of the upper plate constant is proportional to the velocity itself; these fluids are called Newtonian. Fluids for which the force is not proportional to the velocity are called non-Newtonian [Pry66]. A more general definition states that a fluid is Newtonian if the stress exerted is directly proportional to the rate of deformation and does not depend on the deformation itself [Fer91b]; a fluid is non-Newtonian otherwise.

Consider, for simplicity, that the liquid in Figure 2.3 is Newtonian. The velocity of each atom is the sum of two different components; one is due to the thermal motion, the other is due to the streaming velocity of the fluid. For weak to moderate flows, it can be experimentally proved that the streaming velocity (directed in the x -direction) of the fluid varies linearly if measured in the y -direction, from zero at the lower plate to v_0 at the upper one. The fluid is thus said to be in a condition of steady laminar flow with a velocity gradient $\frac{v_0}{L}$ [Pry66]. At steady state, the force F_x^{fluid} per unit area exerted by the fluid in the x -direction on the upper plate is equal (but with opposite sign) to the force F used to drag the plate itself. F_x^{fluid} is related to v_0 by the expression:

$$\frac{F_x^{fluid}}{A} = -\frac{F}{A} = -\mathbf{h} \frac{v_0}{L} \quad (2.58)$$

where \mathbf{h} is the coefficient of shear viscosity, and the negative sign indicates that the force is in the negative x -direction [Pry66].

Considering Eq. (2.58), it becomes convenient to define two quantities that account for the mutually perpendicular directions of the force F_x^{fluid} (x -direction) and of the velocity gradient $\frac{v_0}{L}$ (y -direction):

$$P_{xy} = -\mathbf{h} \frac{\partial v_x}{\partial y} \quad (2.59)$$

where $P_{xy} = \frac{F_x^{fluid}}{A} = -\frac{F}{A}$ is simply the force per unit area exerted by the fluid on the upper plate and it is a negative quantity. The x -subscript represents the direction of the force, whereas the y -subscript is the direction perpendicular to the plate. $\frac{\partial v_x}{\partial y} = \frac{v_0}{L}$ is the velocity gradient (or the strain rate). Here the x -subscript represents the component of the velocity that is not zero, and can only vary in the y -direction. The introduction of these quantities is necessary to describe satisfactorily the system under study, and their experimental measurements allow the calculation of \mathbf{h} via Eq. (2.59).

The upper plate exerts a force $F = -P_{xy}A$ on the adjacent fluid, and during a time Δt it will transfer a momentum equal to $-P_{xy}A\Delta t$. The fluid itself will transfer this momentum to the lower plate with a rate equal to $-\frac{L}{\Delta t}$. This is the x -component of the momentum being transferred along the negative y -direction, ‘layer by layer’ in the fluid. The momentum flow is given by:

$$-P_{xy}A\Delta t \times \left(-\frac{L}{\Delta t} \right) = P_{xy}V \quad (2.60)$$

where V is the volume of the fluid between the plates.

In the following sections we discuss how to treat the momentum flow in Eq. (2.60)

and the strain rate $\frac{\partial v_x}{\partial y}$ within a molecular description.

2.3.2 Pressure and strain rate tensors

Eq (2.60) states that the x -component of momentum flows throughout the fluid, from the upper plate to the lower. Describing a homogeneous fluid as a collection of particles interacting via central forces, the x -component of momentum can be transferred in the y -direction in two ways:

- 1) a particle i with thermal momentum p_{ix} and p_{iy} (x - and y -component respectively),

moves, in an infinitesimal time Δt , a distance $\frac{p_{iy}}{m}\Delta t$ in the y -direction. Hence the

particle transports its own x -component momentum p_{ix} in the y -direction at a rate

$p_{ix} \times \frac{\frac{p_{iy}}{m}\Delta t}{\Delta t} = \frac{p_{ix}p_{iy}}{m}$. This is valid for each particle of the fluid, so adding the

contributions from all the particles, the kinetic contribution to momentum flow is given by:

$$\sum_i \frac{p_{ix}p_{iy}}{m} . \quad (2.61)$$

- 2) The second contribution comes from the intermolecular forces. Let $F(r_{ij})$ be the

magnitude of the (central) force between two particles i and j , where r_{ij} is their

distance apart. The x -component of the force acting on particle j is $F(r_{ij})\frac{x_{ij}}{r_{ij}}$, where

x_{ij} is the distance between i and j in the x -direction. In the time Δt this force will

produce a change in the x -component momentum of particle j equal to $F(r_{ij})\frac{x_{ij}}{r_{ij}}\Delta t$.

Due to Newton's third law of dynamics, particle i experiences an equal change of momentum but of opposite sign. It can be thought that particle j gains momentum

and particle i loses it. If y_{ij} is the distance between the particles in the y -direction,

the velocity with which this momentum transfer occurs is simply $\frac{y_{ij}}{\Delta t}$. Hence the

momentum flow is $F(r_{ij}) \frac{x_{ij}}{r_{ij}} \Delta t \times \frac{y_{ij}}{\Delta t} = F(r_{ij}) \frac{x_{ij} y_{ij}}{r_{ij}}$. Adding the contributions from

all the pairs of particles, the contribution to the momentum flow due to the intermolecular forces can be expressed as:

$$\sum_i \sum_{j>i} F(r_{ij}) \frac{x_{ij} y_{ij}}{r_{ij}} . \quad (2.62)$$

Adding together the contributions from Eq. (2.61) and Eq. (2.62) and using Eq. (2.60), the momentum flow for a homogeneous fluid can be related to the molecular properties as follows [Pry66, Irv50]:

$$P_{xy} V = \sum_i \frac{p_{ix} p_{iy}}{m} + \sum_i \sum_{j>i} F(r_{ij}) \frac{x_{ij} y_{ij}}{r_{ij}} . \quad (2.63)$$

We note here that the above expression is only valid for a homogeneous fluid. The derivation for an inhomogeneous fluid is more complex, but may be found in references [Irv50, Tod95].

Eq. (2.63) can be generalized for any kind of arbitrary flow geometry by writing similar relationships for all the possible combinations of the subscripts (\mathbf{a} , $\mathbf{b}=x, y, z$), which generates a 2nd rank tensor of the form [Pry66]:

$$\mathbf{P} = \begin{pmatrix} P_{xx} & P_{xy} & P_{xz} \\ P_{yx} & P_{yy} & P_{yz} \\ P_{zx} & P_{zy} & P_{zz} \end{pmatrix} . \quad (2.64)$$

Eq. (2.63) is a general relationship, but for a detailed derivation with three-body forces see Appendix 2. Interchanging x and y in Eq. (2.63) it is clear that the tensor \mathbf{P} is

symmetric ($P_{ab} = P_{ba}$). In the equilibrium case the off-diagonal elements are zero (in the kinetic part in Eq. (2.63), p_{ix} and p_{iy} have the same probability to be positive or negative, so the sum of the contributions from all the particles turns out to be zero) and the diagonal elements are all the same. They can be identified as the instantaneous hydrostatic pressure [All87]:

$$P^{eq} \cdot V = \frac{P_{xx}^{eq} + P_{yy}^{eq} + P_{zz}^{eq}}{3} V = NkT + \frac{1}{3} \sum_i \sum_{j>i} \mathbf{F}(r_{ij}) \cdot \mathbf{r}_{ij}. \quad (2.65)$$

It is common practice to use Eq. (2.65) as the definition of hydrostatic pressure also in the non-equilibrium case and to call the tensor \mathbf{P} in Eq. (2.64) the pressure tensor. In general the pressure tensor is a function of temperature, density and strain rate,

$$\mathbf{P} \equiv \mathbf{P} \left(T, \mathbf{r}, \frac{\partial v_x}{\partial y} \right).$$

The strain rate $\frac{\partial v_x}{\partial y}$ can also be defined as a tensor. In general, it represents the

change of the \mathbf{a} -component of the velocity of the fluid in the \mathbf{b} -direction, namely:

$$\frac{\partial v_{\mathbf{a}}}{\partial \mathbf{b}}, \quad \mathbf{a}, \mathbf{b} = x, y, z. \quad (2.66)$$

Considering all the possible combinations of the suffixes, we can write the following tensor, identified as the strain rate tensor:

$$\nabla \mathbf{v} = \begin{pmatrix} \frac{\partial v_x}{\partial x} & \frac{\partial v_y}{\partial x} & \frac{\partial v_z}{\partial x} \\ \frac{\partial v_x}{\partial y} & \frac{\partial v_y}{\partial y} & \frac{\partial v_z}{\partial y} \\ \frac{\partial v_x}{\partial z} & \frac{\partial v_y}{\partial z} & \frac{\partial v_z}{\partial z} \end{pmatrix}. \quad (2.67)$$

For planar Couette flow, the only non-zero element of the tensor in Eq. (2.67) is

$(\nabla \mathbf{v})_{xy} = \frac{\partial v_x}{\partial y}$ which is usually defined by the symbol \mathbf{g} , i.e. the strain rate.

In the following sections we will describe how synthetic NEMD may be used to simulate a planar Couette flow.

2.3.3 Synthetic NEMD for planar Couette flow

Consider a system of N particles interacting via an intermolecular potential $u(\mathbf{r}^1, \dots, \mathbf{r}^N)$ (see for example section 2.1). In a molecular dynamics simulation [All87] one solves Newton's (or Hamiltonian's) equations of motion for each particle:

$$\left. \begin{aligned} \dot{\mathbf{r}}_i &= \frac{d\mathbf{r}_i}{dt} = \frac{\mathbf{p}_i}{m} \\ \dot{\mathbf{p}}_i &= \frac{d\mathbf{p}_i}{dt} = \mathbf{F}_i \end{aligned} \right\} \quad (2.68)$$

where \mathbf{r}_i is the position of particle i , \mathbf{p}_i its momentum and \mathbf{F}_i is the total force acting

on the particle ($\mathbf{F}_i = \sum_{j \neq i}^N \mathbf{F}_{ij} = - \sum_{j \neq i}^N \frac{du_{ij}}{d\mathbf{r}_{ij}}$). Usually periodic boundary conditions

[All87] are applied to simulate bulk properties, since they minimize boundary effects. Several algorithms [All87] can be used to solve the equations of motion in Eq. (2.68); in our (NEMD) simulations we used a fourth-order Gear predictor-corrector method [All87, Eva84b, Gea71, see also below].

In order to calculate transport coefficients, *inhomogeneous* non-equilibrium molecular dynamics techniques try to closely simulate the conditions used in the experimental apparatus to measure the same transport coefficients [Lie92]. To maintain the system under non-equilibrium steady state flow, these techniques adopt boundary conditions (for example sliding walls) which, unfortunately, affect the transport properties of the fluid because the size of the simulated system is comparable with the range of the interatomic interactions [Lie92, Tod95]. For these reasons synthetic algorithms [Eva90], which use fictitious forces, were implemented to maintain the

system in a homogeneous non-equilibrium steady state. The fictitious forces continuously exert work on the system to prevent relaxation to equilibrium. This work causes a heating of the system, which must be removed by a thermostat. Fictitious forces and thermostats are introduced by modifying the Newtonian equations of motion. In what follows we describe how the synthetic NEMD SLLOD method [Eva84c, Eva90], used in our work, re-casts the equations of motion to simulate planar Couette flow.

SLLOD equations of motion

Consider a canonical ensemble of N particles at temperature T . The distribution function is:

$$f_0 = \frac{e^{-H_0/kT}}{\int e^{-H_0/kT} d\mathbf{r}^1 \dots d\mathbf{r}^N d\mathbf{p}^1 \dots d\mathbf{p}^N} \quad (2.69)$$

where

$$H_0 = H_0(\mathbf{r}^1, \dots, \mathbf{r}^N, \mathbf{p}^1, \dots, \mathbf{p}^N) = \sum_{i=1}^N \frac{\mathbf{p}_i \cdot \mathbf{p}_i}{2m} + u(\mathbf{r}^1, \dots, \mathbf{r}^N). \quad (2.70)$$

H_0 is seen to be the total internal energy of the system.

Consider now the instant at which the system is subject to a linear velocity profile. At time $t=0$ the distribution function is changed to the local distribution function

$$f_l = \frac{\exp\left[\frac{-1}{kT} \left(\sum_{i=1}^N \frac{(\mathbf{p}_i + \hat{\mathbf{x}}m\dot{\mathbf{y}}_i) \cdot (\mathbf{p}_i + \hat{\mathbf{x}}m\dot{\mathbf{y}}_i)}{2m} + u(\mathbf{r}^1, \dots, \mathbf{r}^N) \right)\right]}{\int \exp\left[\frac{-1}{kT} \left(\sum_{i=1}^N \frac{(\mathbf{p}_i + \hat{\mathbf{x}}m\dot{\mathbf{y}}_i) \cdot (\mathbf{p}_i + \hat{\mathbf{x}}m\dot{\mathbf{y}}_i)}{2m} + u(\mathbf{r}^1, \dots, \mathbf{r}^N) \right)\right] d\mathbf{r}^1 \dots d\mathbf{p}^N} \quad (2.71)$$

($\hat{\mathbf{x}}$: x -direction unit vector)

by transforming the x -component of the velocity of each particle, imposing a linear velocity profile [Eva84c, Eva90]:

$$\dot{x}_i(0^+) = \dot{x}_i(0^-) + \dot{\mathbf{g}}y_i . \quad (2.72)$$

This is a canonical ensemble (locally in equilibrium) upon which is superimposed a linear velocity profile with strain rate $\dot{\mathbf{g}} = dv_x/dy$ (zero-wave-vector strain rate [Eva90]). It is important to realize that f_l is simply a local equilibrium distribution function, i.e. molecular relaxation has not yet taken place. The distribution function of this ensemble can be obtained by considering the response of a canonical ensemble f_0 at $t=0$ to a fictitious strain rate field $\dot{\mathbf{g}}(t)$ where the system evolves with the following equations of motion [Eva84c]:

$$\left. \begin{aligned} \ddot{x}_i &= F_{ix}/m + \dot{\mathbf{g}}(t)y_i \\ \ddot{y}_i &= F_{iy}/m \\ \ddot{z}_i &= F_{iz}/m \end{aligned} \right\} \text{with } \left. \begin{aligned} \dot{\mathbf{g}}(t) &= 0 \quad \text{for } t < 0 \\ \dot{\mathbf{g}}(t) &= \dot{\mathbf{g}} \quad \text{for } t \geq 0 \end{aligned} \right\} \quad (2.73)$$

Eq. (2.73) are equivalent to the following first-order equations of motions:

$$\left. \begin{aligned} \dot{x}_i &= p_{ix}/m + \dot{\mathbf{g}}y_i \\ \dot{y}_i &= p_{iy}/m \\ \dot{z}_i &= p_{iz}/m \end{aligned} \right\} \quad (2.74)$$

$$\left. \begin{aligned} \dot{p}_{ix} &= F_{ix} - \dot{\mathbf{g}}p_{iy} \\ \dot{p}_{iy} &= F_{iy} \\ \dot{p}_{iz} &= F_{iz} \end{aligned} \right\} . \quad (2.75)$$

It is important to point out that Eq. (2.74) and Eq. (2.75) can not be derived from a Hamiltonian. p_{ix} is the peculiar (thermal) momentum ($p_{ix}^{tot.} - p_{ix}^{stream. vel.}$) rather than the laboratory momentum.

The shear viscosity is defined as:

$$\mathbf{h} = -\frac{1}{\dot{\mathbf{g}}} \langle P_{xy} \rangle_{t \rightarrow \infty} = -\frac{1}{2\dot{\mathbf{g}}} \langle P_{xy} + P_{yx} \rangle_{t \rightarrow \infty} \quad (2.76)$$

where $\langle \rangle_{t \rightarrow \infty}$ represents a time average on the dynamics of the system.

Differentiating H_0 in Eq. (2.70), and using Eqs. (2.74), (2.75) and (2.63) we have the following equation:

$$\dot{H}_0 = -\dot{\mathbf{g}} \cdot \mathbf{p}_{xy} V \quad (2.77)$$

which states that the work exerted by the external field in an *adiabatic* planar Couette flow results in a change of the internal energy. As a consequence, the system heats up. This behaviour is revealed by an increase of the kinetic energy, where as usual, the kinetic energy is identified with the kinetic temperature as:

$$\frac{3}{2} NkT = \sum_{i=1}^N \frac{\mathbf{p}_i \cdot \mathbf{p}_i}{2m} . \quad (2.78)$$

Since we want to simulate Couette flow at constant temperature, we need to introduce a thermostat in the equations of motion. For this purpose Eq. (2.75) is re-written as:

$$\left. \begin{aligned} \dot{p}_{ix} &= F_{ix} - \dot{\mathbf{g}} p_{iy} - \mathbf{a} p_{ix} \\ \dot{p}_{iy} &= F_{iy} - \mathbf{a} p_{iy} \\ \dot{p}_{iz} &= F_{iz} - \mathbf{a} p_{iz} \end{aligned} \right\} \quad (2.79)$$

where \mathbf{a} is a Gaussian thermostating multiplier [Eva90] derived by constraining the kinetic energy (hence the temperature) to be constant:

$$\frac{dT}{dt} = 0 \Rightarrow \frac{d \left(\sum_{i=1}^N \frac{\mathbf{p}_i \cdot \mathbf{p}_i}{2m} \right)}{dt} = 0 \Rightarrow \mathbf{a} = \frac{\sum_{i=1}^N (\mathbf{F}_i \cdot \mathbf{p}_i - \dot{\mathbf{g}} p_{ix} p_{iy})}{\sum_{i=1}^N \mathbf{p}_i \cdot \mathbf{p}_i} . \quad (2.80)$$

In Eqs. (2.74), (2.79) and (2.80) it is assumed that the linear velocity profile is stable, which is true at low Reynolds number [Eva90].

The SLLOD equations of motions must be implemented with compatible periodic boundary conditions [Eva90]. For planar Couette flow (Eq. (2.74) and Eq. (2.79)), Lees-

Edwards boundary conditions [All87, Eva90] can be used. In the next section we give some details of these boundary conditions.

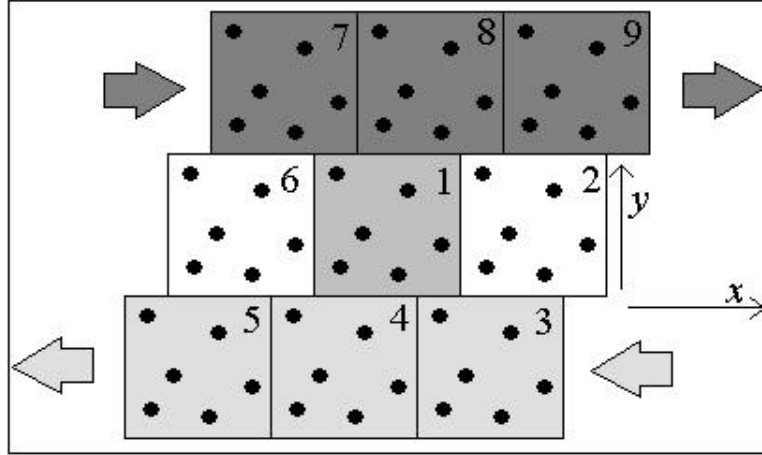


Figure 2.4 Representation of the Lees-Edwards boundary conditions [All87, Eva90].

Lees-Edwards boundary conditions

Figure 2.4 depicts an infinite periodic system subjected to shear in the x - y plane. Box 1 is the simulation box. The boxes in the middle layer (2, 1 and 6) are stationary. Boxes in the lower layer (3, 4 and 5) move in the negative x -direction at a speed $\dot{\mathbf{g}}L$, where L is the length of the (cubic) box. The boxes in the upper layer (7, 8 and 9) move in the positive x -direction at a speed $\dot{\mathbf{g}}L$. At each step of the simulation the relative distances (x_{ij} , y_{ij} and z_{ij}) between pairs of particles i and j are calculated with Lees-Edwards boundary conditions [All87, Eva90] in the following way:

$$\begin{aligned}
 x_{ij} &\leftarrow x_{ij} - dx_d \times \text{anint}(y_{ij}/L) \times L \\
 x_{ij} &\leftarrow x_{ij} - \text{anint}(x_{ij}/L) \times L \\
 y_{ij} &\leftarrow y_{ij} - \text{anint}(y_{ij}/L) \times L \\
 z_{ij} &\leftarrow z_{ij} - \text{anint}(z_{ij}/L) \times L
 \end{aligned} \tag{2.81}$$

In Eq. (2.81)

$$dx_d = \text{mod}(\dot{\mathbf{g}} \times t_{el}; L) , \tag{2.82}$$

where $\text{mod}(a ; b)$ is a function that returns the remainder of the division of b into a and t_{el} is time elapsed during the simulation. $\text{anint}(a)$ is a function that returns the nearest integer to a .

It is convenient to replace particles in the simulation box as they cross the boundaries. After each step of the simulation, the following algorithm (similar to Eq. (2.81)) must be used for the coordinates (x_i, y_i, z_i) of the particles:

$$\begin{aligned} x_i &\leftarrow x_i - dx d \times \text{anint}(y_i / L) \times L \\ x_i &\leftarrow x_i - \text{anint}(x_i / L) \times L \\ y_i &\leftarrow y_i - \text{anint}(y_i / L) \times L \\ z_i &\leftarrow z_i - \text{anint}(z_i / L) \times L \end{aligned} \quad (2.83)$$

where we note that the origin of the coordinate system is the centre of the simulation box. If the particle crosses the lower x - z face of the simulation box it will ‘reappear’ at the upper x - z face, and the streaming velocity (\mathbf{gL}) will be added to its total velocity. If it crosses the upper x - z face reappearing in the lower x - z face, the streaming velocity (\mathbf{gL}) will be subtracted from its total velocity. In the other cases the total velocity is not changed.

Gear predictor-corrector method

To solve the first-order SLLOD equations of motion (Eqs. (2.74) and (2.79)), we used a fourth-order Gear predictor-corrector method [All87, Eva84b, Gea71] for its efficiency and accuracy. Despite its 4th order accuracy it requires only first derivatives of the intermolecular potential which is calculated once per time-step. Let \mathbf{r}_i be the position of particle i , the scaled time derivatives can be defined as:

$$\mathbf{r}_{1i} = \Delta t \left(\frac{d\mathbf{r}_i}{dt} \right) ; \mathbf{r}_{2i} = \frac{1}{2} \Delta t^2 \left(\frac{d^2\mathbf{r}_i}{dt^2} \right) ; \mathbf{r}_{3i} = \frac{1}{6} \Delta t^3 \left(\frac{d^3\mathbf{r}_i}{dt^3} \right) ; \mathbf{r}_{4i} = \frac{1}{24} \Delta t^4 \left(\frac{d^4\mathbf{r}_i}{dt^4} \right) \quad (2.84)$$

where Δt is the time step. Equivalently for the momentum \mathbf{p}_i , we have:

$$\mathbf{p}_{1i} = \Delta t \left(\frac{d\mathbf{p}_i}{dt} \right) ; \mathbf{p}_{2i} = \frac{1}{2} \Delta t^2 \left(\frac{d^2 \mathbf{p}_i}{dt^2} \right) ; \mathbf{p}_{3i} = \frac{1}{6} \Delta t^3 \left(\frac{d^3 \mathbf{p}_i}{dt^3} \right) ; \mathbf{p}_{4i} = \frac{1}{24} \Delta t^4 \left(\frac{d^4 \mathbf{p}_i}{dt^4} \right) \quad (2.85)$$

The Taylor series expansion for \mathbf{r}_i and \mathbf{p}_i is truncated at the 4th order, and using a matrix form we can write the predicted values (superscript p) of \mathbf{r}_i and \mathbf{p}_i and their derivatives in the following way:

$$\begin{pmatrix} \mathbf{r}_i^p(t + \Delta t) \\ \mathbf{r}_{i1}^p(t + \Delta t) \\ \mathbf{r}_{i2}^p(t + \Delta t) \\ \mathbf{r}_{i3}^p(t + \Delta t) \\ \mathbf{r}_{i4}^p(t + \Delta t) \end{pmatrix} = \begin{pmatrix} 1 & 1 & 1 & 1 & 1 \\ 0 & 1 & 2 & 3 & 4 \\ 0 & 0 & 1 & 3 & 6 \\ 0 & 0 & 0 & 1 & 4 \\ 0 & 0 & 0 & 0 & 1 \end{pmatrix} \begin{pmatrix} \mathbf{r}_i(t) \\ \mathbf{r}_{i1}(t) \\ \mathbf{r}_{i2}(t) \\ \mathbf{r}_{i3}(t) \\ \mathbf{r}_{i4}(t) \end{pmatrix} \quad (2.86)$$

$$\begin{pmatrix} \mathbf{p}_i^p(t + \Delta t) \\ \mathbf{p}_{1i}^p(t + \Delta t) \\ \mathbf{p}_{2i}^p(t + \Delta t) \\ \mathbf{p}_{3i}^p(t + \Delta t) \\ \mathbf{p}_{4i}^p(t + \Delta t) \end{pmatrix} = \begin{pmatrix} 1 & 1 & 1 & 1 & 1 \\ 0 & 1 & 2 & 3 & 4 \\ 0 & 0 & 1 & 3 & 6 \\ 0 & 0 & 0 & 1 & 4 \\ 0 & 0 & 0 & 0 & 1 \end{pmatrix} \begin{pmatrix} \mathbf{p}_i(t) \\ \mathbf{p}_{1i}(t) \\ \mathbf{p}_{2i}(t) \\ \mathbf{p}_{3i}(t) \\ \mathbf{p}_{4i}(t) \end{pmatrix} \quad (2.87)$$

When the predicted values are calculated, Lees-Edwards periodic boundary conditions (Eq. (2.83)) are applied to reintroduce particles into the simulation box, which may have crossed the boundaries. The relative distances between pairs of particles are first calculated by Eq. (2.81) and then used to determine the forces acting on each atom. Finally, Eq. (2.74) and Eq. (2.79) are used in the corrector step to calculate the corrected values (superscript c) of \mathbf{r}_i and \mathbf{p}_i and their derivatives:

$$\begin{pmatrix} \mathbf{r}_i^c(t + \Delta t) \\ \mathbf{r}_{i1}^c(t + \Delta t) \\ \mathbf{r}_{i2}^c(t + \Delta t) \\ \mathbf{r}_{i3}^c(t + \Delta t) \\ \mathbf{r}_{i4}^c(t + \Delta t) \end{pmatrix} = \begin{pmatrix} \mathbf{r}_i^p(t + \Delta t) \\ \mathbf{r}_{i1}^p(t + \Delta t) \\ \mathbf{r}_{i2}^p(t + \Delta t) \\ \mathbf{r}_{i3}^p(t + \Delta t) \\ \mathbf{r}_{i4}^p(t + \Delta t) \end{pmatrix} + \Delta \mathbf{r}_i \begin{pmatrix} c_0 \\ c_1 \\ c_2 \\ c_3 \\ c_4 \end{pmatrix} \quad (2.88)$$

$$\begin{pmatrix} \mathbf{p}_i^c(t + \Delta t) \\ \mathbf{p}_{i1}^c(t + \Delta t) \\ \mathbf{p}_{i2}^c(t + \Delta t) \\ \mathbf{p}_{i3}^c(t + \Delta t) \\ \mathbf{p}_{i4}^c(t + \Delta t) \end{pmatrix} = \begin{pmatrix} \mathbf{p}_i^p(t + \Delta t) \\ \mathbf{p}_{i1}^p(t + \Delta t) \\ \mathbf{p}_{i2}^p(t + \Delta t) \\ \mathbf{p}_{i3}^p(t + \Delta t) \\ \mathbf{p}_{i4}^p(t + \Delta t) \end{pmatrix} + \Delta \mathbf{p}_i \begin{pmatrix} c_0 \\ c_1 \\ c_2 \\ c_3 \\ c_4 \end{pmatrix} \quad (2.89)$$

where:

$$\Delta \mathbf{r}_i = \begin{pmatrix} x_{li} - (p_{ix} + \dot{\mathbf{g}}_i) \Delta t \\ y_{li} - p_{iy} \Delta t \\ z_{li} - p_{iz} \Delta t \end{pmatrix} \quad (2.90)$$

$$\Delta \mathbf{p}_i = \begin{pmatrix} p_{lix} - (F_{ix} - \mathbf{a}p_{ix} - \dot{\mathbf{g}}_i) \Delta t \\ p_{liy} - (F_{iy} - \mathbf{a}p_{iy}) \Delta t \\ p_{liz} - (F_{iz} - \mathbf{a}p_{iz}) \Delta t \end{pmatrix}. \quad (2.91)$$

Here c_0 , c_1 , c_2 , c_3 and c_4 are the corrector coefficients which depend upon the order of the differential equation being solved [Gea71]. In our case, $c_0=251/720$, $c_1=1$, $c_2=11/12$, $c_3=1/3$ and $c_4=1/24$.

Other methods can be used to integrate equations of motion of the particles. The commonly used leap frog method [Ver67] solves second order equations of motion, hence it is not suitable to solve first order Eqs. (2.74) and (2.79). The Runge-Kutta method [Gea71] is appropriate but expensive computationally. We have chosen to use the fourth-order Gear predictor-corrector method for its good accuracy and because of programming convenience.

2.3.4 Non-equilibrium pair distribution functions

Given a canonical ensemble (NVT), where the origin of the coordinate system is arbitrarily chosen, it is possible to define distribution functions for the particle positions. The simplest such function is the pair (2^{nd} order) distribution function $g(\mathbf{r}_1, \mathbf{r}_2)$. In a homogeneous atomic fluid, it is proportional to the probability of finding a particle at \mathbf{r}_2

in a volume element $d\mathbf{r}_2$ if, at the same time, there is a particle at \mathbf{r}_1 in volume $d\mathbf{r}_1$ [Ege94]. This function is useful since it can be easily calculated from a molecular simulation, providing insight into the liquid structure. It can also be measured experimentally [Ege94], allowing a direct comparison between theory and experiment. Furthermore, the pair distribution function, when known, provides an alternative way to calculate any pair function of the system, such as the two-body configurational pressure, energy and viscosity. Hence it can be used to test the correctness of those pair functions calculated directly from a molecular simulation. Higher order distribution functions can be defined in a similar way [Ege94].

For a homogeneous liquid in thermal equilibrium or under steady state uniform flow, $g(\mathbf{r}_1, \mathbf{r}_2)$ does not depend upon the choice of the origin of the coordinates [Ege94]. Hence $g(\mathbf{r}_1, \mathbf{r}_2)$ depends upon the difference $\mathbf{r} = \mathbf{r}_1 - \mathbf{r}_2$ and can be defined as an ensemble average over all possible pairs [All87]:

$$g(\mathbf{r}) = \frac{V}{N^2} \left\langle \sum_{i=1}^N \sum_{j>i}^N \mathbf{d}(\mathbf{r} - \mathbf{r}_{ij}) \right\rangle \quad (2.92)$$

where $\mathbf{d}(\mathbf{r} - \mathbf{r}_{ij})$ is the delta function. Further, for an isotropic liquid $g(\mathbf{r})$ depends only upon the magnitude of \mathbf{r} , so it is a spherically symmetrical function. In this case $g(\mathbf{r})$ is easily calculated as:

$$g(r) = \frac{\langle N_r \rangle}{4\pi r^2 dr} \quad (2.93)$$

where $\langle N_r \rangle$ is the average number of particles between a spherical shell of radius r and thickness dr . In planar Couette flow $g(\mathbf{r})$ is not a spherically symmetrical function and can be approximated as [Gre52, Han80]:

$$g(\mathbf{r}) = g(r) + \dot{\mathbf{g}} \mathbf{n}(r) \sin^2 \mathbf{q} \sin \mathbf{f} \cos \mathbf{f} \quad (2.94)$$

where we use the polar coordinates:

$$\left. \begin{aligned} x &= r \sin \mathbf{q} \cos \mathbf{f} \\ y &= r \sin \mathbf{q} \sin \mathbf{f} \\ z &= r \cos \mathbf{q} \end{aligned} \right\}. \quad (2.95)$$

In Eq. (2.94), $g(r)$ is the standard radial distribution function (Eq. 2.93). In this work we have calculated this quantity for a system in equilibrium and for planar Couette flow (see Chapter 4). The function $\mathbf{n}(r)$ represents the purely radial part of the distortion and it can be estimated by the expression [Han80]:

$$\mathbf{n}(r) = \frac{15}{8\mathbf{p}} \frac{1}{\mathbf{g}\mathbf{r}} \frac{1}{r^2} \frac{dr}{dr} \left\langle \frac{x_{ij} y_{ij}}{r_{ij}^2} \right\rangle \quad (2.96)$$

where $\left\langle \frac{x_{ij} y_{ij}}{r_{ij}^2} \right\rangle$ is the average of the quantity $\frac{x_{ij} y_{ij}}{r_{ij}^2}$ for each particle contained in a spherical shell of radius r and thickness dr . We have calculated $\mathbf{n}(r)$ for planar Couette flow (see Chapter 4). For a system in equilibrium $\mathbf{n}(r)$ is zero.

In what follows we give the expressions of the two-body potential contributions to the pressure, energy and viscosity in terms of $g(r)$ and $\mathbf{n}(r)$.

Two-body potential pressure, energy and viscosity as functions of $g(r)$ and $\mathbf{n}(r)$

The two-body potential contribution for the pressure can be written as [All87]:

$$\begin{aligned} P^{2b} &= \frac{1}{3V} \sum_{i=1}^N \sum_{j>i}^N (F_{ix}^{2b} x + F_{iy}^{2b} y + F_{iz}^{2b} z) = \\ &= \frac{1}{3V} \sum_{i=1}^N \sum_{j>i}^N \left(-\frac{x}{r} \frac{du^{2b}}{dr} x - \frac{y}{r} \frac{du^{2b}}{dr} y - \frac{z}{r} \frac{du^{2b}}{dr} z \right) = -\frac{1}{3V} \sum_{i=1}^N \sum_{j>i}^N \left(r \frac{du^{2b}}{dr} \right). \end{aligned} \quad (2.97)$$

Using Eq. (2.92) and Eq.(2.94) we can write:

$$\begin{aligned}
P^{2b} &= -\frac{1}{3} \frac{\mathbf{r}^2}{2} \int g(\mathbf{r}) r \frac{du^{2b}}{dr} r^2 \sin \mathbf{q} d\mathbf{q} d\mathbf{f} dr = \\
& -\frac{\mathbf{r}^2}{6} \int (g(r) + \dot{\mathbf{g}} \mathbf{n}(r) \sin^2 \mathbf{q} \sin \mathbf{f} \cos \mathbf{f}) \frac{du^{2b}}{dr} r^3 \sin \mathbf{q} d\mathbf{q} d\mathbf{f} dr = \\
& -\frac{\mathbf{r}^2}{6} \int g(r) \frac{du^{2b}}{dr} r^3 \sin \mathbf{q} d\mathbf{q} d\mathbf{f} dr - \\
& \frac{\mathbf{r}^2}{6} \int \dot{\mathbf{g}} \mathbf{n}(r) \sin^2 \mathbf{q} \sin \mathbf{f} \cos \mathbf{f} \frac{du^{2b}}{dr} r^3 \sin \mathbf{q} d\mathbf{q} d\mathbf{f} dr
\end{aligned} \tag{2.98}$$

where:

$$-\frac{\mathbf{r}^2}{6} \int \dot{\mathbf{g}} \mathbf{n}(r) \sin^2 \mathbf{q} \sin \mathbf{f} \cos \mathbf{f} \frac{du^{2b}}{dr} r^3 \sin \mathbf{q} d\mathbf{q} d\mathbf{f} dr = 0 \tag{2.99}$$

since:
$$\int_0^{2p} \sin \mathbf{f} \cos \mathbf{f} d\mathbf{f} = 0 \quad . \tag{2.100}$$

Hence:

$$P^{2b} = -\frac{\mathbf{r}^2}{6} \int g(r) \frac{du^{2b}}{dr} r^3 \sin \mathbf{q} d\mathbf{q} d\mathbf{f} dr = -\frac{2p\mathbf{r}^2}{3} \int_0^\infty g(r) \frac{du^{2b}}{dr} r^3 dr \quad . \tag{2.101}$$

Equivalently for the two-body potential energy we can write:

$$E^{2b} = 2pN\mathbf{r} \int_0^\infty g(r) u^{2b} r^2 dr \quad . \tag{2.102}$$

Eq. (2.101) and Eq. (2.102) state that P^{2b} and E^{2b} do not depend on the radial part of the distortion, $\mathbf{n}(r)$, and the only dependence on the shear rate $\dot{\mathbf{g}}$ comes from the distortion of $g(r)$ under shear (since $g(r)^{equil.} \neq g(r)^{non-equil.}$). Following the same procedure we can write a similar expression for the 2-body potential shear contribution to the viscosity which depends only on $\mathbf{n}(r)$:

$$\mathbf{h}^{2b} = \frac{2p\mathbf{r}^2}{15} \int_0^\infty \mathbf{n}(r) \frac{du^{2b}}{dr} r^3 dr \quad . \tag{2.103}$$